Human CD34+ Hematopoietic Stem Cell–Engrafted NSG Mice: Morphological and Immunophenotypic Features

Blümich, Sandra ; Zdimerova, Hana ; Münz, Christian ; Kipar, Anja ; Pellegrini, Giovanni

Abstract: Immunodeficient mice engrafted with human immune cells represent an innovative tool to improve translatability of animal models for the study of human diseases. Immunophenotyping in these mice focuses on engraftment rates and cellular differentiation in blood and secondary lymphoid organs, and is predominantly carried out by FACS (fluorescent activated cell sorting) analysis; information on the morphological aspects of engraftment and the prevalence of histologic lesions is limited. We histologically examined 3- to 6-month-old NSG mice, naïve or engrafted with CD34+ human hemopoietic stem cells (HSC), and employed a quantitative immunohistochemical approach to identify human and murine cell compartments, comparing the results with the FACS data. NSG mice mainly exhibited incidental findings in lungs, kidneys, testes, and adrenal glands. A 6-month-old NSG mouse had a mediastinal lymphoblastic lymphoma. The lymphoid organs of NSG mice lacked typical lymphoid tissue architecture but frequently exhibited small periarteriolar leukocyte clusters in the spleen. Mice engrafted with human HSC frequently showed nephropathy, ovarian atrophy, cataract, and abnormal retinal development, lesions considered secondary to irradiation. In addition, 20% exhibited multisystemic granulomatous inflammatory infiltrates, dominated by human macrophages and T cells, leading to the observed 7% mortality and morbidity. Immunophenotypic data revealed variable repopulation of lymphoid organs with hCD45+ human cells, which did not always parallel the engraftment levels measured via FACS. The study describes the most common pathological features in young NSG mice after human HSC engraftment. As some of these lesions contribute to morbidity, morphological assessment of the engraftment at tissue level might help improve immunophenotypic evaluations of this animal model.

DOI: https://doi.org/10.1177/0300985820948822

Veterinary Pathology

Human CD34+ hematopoietic stem cell-engrafted NSG mice: Morphological and immunophenotypic features

Journal:	*Veterinary Pathology*
Manuscript ID	VET-19-FLM-0283.R3
Manuscript Type:	Full Length Manuscript
Date Submitted by the Author:	n/a
Complete List of Authors:	Blümich, Sandra; University of Zurich, Institute of Veterinary Pathology Zdimerova, Hana; University of Zurich, Institute of Experimental Immunology Münz, Christian; University of Zurich, Institute of Experimental Immunology Kipar, Anja; University of Zurich, Institute of Veterinary Pathology; University of Liverpool, Institute of Global Health Pellegrini, Giovanni; University of Zurich, Institute of Veterinary Pathology
Keywords:	NSG mice, CD34+ stem cells, engraftment, humanized mice, graft versus host disease, lymphoma, non-obese diabetic mice, granulomatous inflammation
Abstract:	Immunodeficient mice engrafted with human immune cells represent an innovative tool to improve translatability of animal models for the study of human diseases. Immunophenotyping in these mice focuses on engraftment rates and cellular differentiation in blood and secondary lymphoid organs, and is predominantly carried out by FACS analysis; information on the morphological aspects of engraftment and the prevalence of histologic lesions is limited. We histologically examined 3-6-month-old NSG mice, naïve or engrafted with CD34+ human hemopoietic stem cells (HSC), and employed a quantitative immunohistochemical approach to identify human and murine cell compartments, comparing the results with the FACS data. NSG mice mainly exhibited incidental findings in lungs, kidneys, testes and adrenal glands. A 6-month-old NSG mouse had a mediastinal lymphoblastic lymphoma. The lymphoid organs of NSG mice lacked typical lymphoid tissue architecture but frequently exhibited small periarteriolar leukocyte clusters in the spleen. Mice engrafted with human HSC frequently showed nephropathy, ovarian atrophy, cataract and abnormal retinal development, lesions considered secondary to irradiation. In addition, 20% exhibited multisystemic granulomatous inflammatory infiltrates, dominated by human macrophages and T cells, leading to the observed 7% mortality and morbidity. Immunophenotypic data revealed variable repopulation of lymphoid organs with hCD45+ human cells, which did not always parallel the engraftment levels measured via FACS. The study describes the most common pathological features in young

	NSG mice after human HSC engraftment. As some of these lesions contribute to morbidity, morphological assessment of the engraftment at tissue level might help improve immunophenotypic evaluations of this animal model.

Human CD34$^+$ hematopoietic stem cell-engrafted NSG mice: Morphological and immunophenotypic features

Sandra Blümich, Hana Zdimerova, Christian Münz, Anja Kipar, Giovanni Pellegrini

Laboratory for Animal Model Pathology (LAMP), Institute of Veterinary Pathology, Vetsuisse Faculty, University of Zurich, Zurich, Switzerland (SB, AK, GP)
Viral Immunobiology, Institute of Experimental Immunology, University of Zurich, Zurich, Switzerland (HZ, CM)

Corresponding author:
Anja Kipar
Institute of Veterinary Pathology
Vetsuisse Faculty
University of Zurich
Winterthurerstrasse 268
CH - 8057 Zurich
Switzerland
Phone: 41 44 635 85 51
Fax: +41 44 6358934
E-mail address: anja.kipar@uzh.ch

Abstract

Immunodeficient mice engrafted with human immune cells represent an innovative tool to improve translatability of animal models for the study of human diseases. Immunophenotyping in these mice focuses on engraftment rates and cellular differentiation in blood and secondary lymphoid organs, and is predominantly carried out by FACS analysis; information on the morphological aspects of engraftment and the prevalence of histologic lesions is limited.

We histologically examined 3-6-month-old NSG mice, naïve or engrafted with $CD34^+$ human hemopoietic stem cells (HSC), and employed a quantitative immunohistochemical approach to identify human and murine cell compartments, comparing the results with the FACS data.

NSG mice mainly exhibited incidental findings in lungs, kidneys, testes and adrenal glands. A 6-month-old NSG mouse had a mediastinal lymphoblastic lymphoma. The lymphoid organs of NSG mice lacked typical lymphoid tissue architecture but frequently exhibited small periarteriolar leukocyte clusters in the spleen. Mice engrafted with human HSC frequently showed nephropathy, ovarian atrophy, cataract and abnormal retinal development, lesions considered secondary to irradiation. In addition, 20% exhibited multisystemic granulomatous inflammatory infiltrates, dominated by human macrophages and T cells, leading to the observed 7% mortality and morbidity. Immunophenotypic data revealed variable repopulation of lymphoid organs with $hCD45^+$ human cells, which did not always parallel the engraftment levels measured via FACS.

The study describes the most common pathological features in young NSG mice after human HSC engraftment. As some of these lesions contribute to morbidity, morphological assessment of the engraftment at tissue level might help improve immunophenotypic evaluations of this animal model.

Keywords: NSG mice, non-obese diabetic mice, Prkdc^{scid}, IL-2Rγ^{nul}, CD34^{+} stem cells, engraftment, humanized mice, granulomatous inflammation, graft versus host disease, lymphoma, radiation nephropathy.

Recent advances in the generation of humanized murine models, featuring immunodeficient mice engrafted with human immune system cells, have brought tangible breakthroughs in numerous research fields, such as the preclinical development of immunotherapeutic agents and the study of infectious, metabolic and autoimmune diseases. Progress has been facilitated by the optimisation of immunodeficient mouse models, which, being deprived of acquired and innate immunity, can be transplanted with human cells that eventually develop into a variably functional immune system in the model.[9,45,57,61]

Among the numerous immunodeficient mouse strains available, the NOD-scid IL-2Rγ^{null} (NSG) mouse is currently the most widely used for successful humanization of the immune system, showing one of the highest engraftment rates among the various strains.[29,64] NSG mice are non-obese diabetic (NOD) mice bearing the Prkdc^{scid} mutation and a genetic deletion of the common γ chain of the IL-2 receptor. Accordingly, they exhibit defects in lymphoid cell development, lacking both innate and adaptive lymphocytes, and have diminished complement activity due to C5 deficiency.[9,24,52] In contrast to their NOD/scid predecessors, NSG mice are not prone to develop thymic lymphoma; they have a long life span of about two years.[9,23] Functional immune system abnormalities in immunodeficient mice are associated with abnormal development of the primary and secondary lymphoid organs; however, the morphological equivalents of the latter vary across the available models.[49] NSG mice, for example, exhibit a small spleen, thymus and lymph nodes that lack lymphoid structures and are composed almost exclusively of reticular stromal cells.[47,51,52]

Immunodeficient mice can be transiently or stably humanized by administration of human mature lymphoid or CD34^{+} hematopoietic stem cells (HSC), respectively.[61] Most models allow multi-lineage human immune cell engraftment and both the

acquired and innate human immune system components develop to variable degrees. The present study focuses on CD34$^+$ HSC humanized NSG (hu-NSG) mice, a model in which T and B cell engraftment is generally successful, though without consistent immunoglobulin (Ig) class switching and mostly IgM production by B cells.[19,45,56] Hu-NSG mice have human dendritic cells, NK cells and myeloid cells including neutrophils.[25,35,60] However, the latter two are generally seen at low numbers, and seem to be defective in their maturation and function.[19,23,45,57] It has been shown that the transplanted human leukocytes form variably sized aggregates in the lymphoid organs of these mice, which in general do not exhibit distinctive secondary lymphoid structures such as lymphoid follicles in spleen and lymph nodes.[23,57,60] In the thymus, repopulation appears to be more efficient in immunodeficient mice transplanted shortly after birth, whilst in mice engrafted at adult age the thymus is less prone to support human cell engraftment.[7,62] In the bone marrow the proportion of lymphoid and myeloid cells varies, as different published studies indicate.[60,62]

Effective engraftment in hu-NSG mice is generally determined by fluorescent activated cell sorting (FACS) analysis of the blood, usually at 12-16 weeks post-engraftment. The FACS data suggest that the extent of engraftment can vary substantially depending on the age of the mice, the source and manipulation of the HSC, and the administration route.[23,26] So far, most of the immunophenotyping data that are available for these mice are based on FACS analyses, carried out on circulating and organ-specific immune cells at different endpoints.[7,26,39,56] Accordingly, there is very limited information concerning the *in situ* aspects of engraftment, in particular in the hemolymphatic tissues and, specifically, how these correlate with the engraftment rates and cellular differentiation determined by FACS. Furthermore, little is known about the incidence of spontaneous diseases and

common histopathological lesions in hu-NSG mice, and even in NSG mice. Information about the spectrum of histopathological lesions occurring spontaneously in NSG mice is mainly limited to the prevalence of neoplastic findings in the NOD background strain[22] or a few reports on the most common causes of mortality and morbidity and age-related lesions in old NSG mice housed in conventional mouse facilities.[16,47] In the few reports available about hu-NSG mice, spontaneous changes were generally mentioned alongside the findings relevant to the study instead of being a focus of investigation.[8,32,47,62] However, a recent study reported histological lesions that provide evidence of the occurrence of graft versus host disease (GvHD) in HSC hu-NSG mice.[11] Considering the increasing use of humanized mice in efficacy and safety studies, including regulatory safety assessment, this knowledge gap needs to be addressed and better characterization of the model is warranted to consolidate its translatability.

The present study aimed to characterize the morphological phenotype of NSG mice and their humanized counterpart, the CD34$^+$ hu-NSG murine model generated via perinatal intrahepatic injection of human CD34$^+$ fetal liver cells into NSG mice after preconditioning irradiation. We found high variability in the levels of human cell engraftment in the blood of hu-NSG mice within the same experiment and hypothesized that this is reflected by a similarly variable reconstitution in the lymphoid organs. Another purpose of this study was to assess the spectrum of histopathological lesions and identify the main causes of morbidity and mortality in young NSG and CD34$^+$ HSC hu-NSG mice, since, despite the increased popularity of these animal models in nonclinical testing, the published data on this topic is very sparse.

.

Materials and Methods

Animals

The study was undertaken on NOD-scid IL-2Rγ^{null} (NSG) mice from a breeding colony established in a research facility at the Institute of Experimental Immunology, University of Zurich, Switzerland from animals originally purchased from Jackson Laboratories (Bar Harbor, USA). Animals were housed in groups of up to five males or females respectively and fed *ad libitum* with conventional diet (M/R Haltung Extrudat, Alleinfuttermittel für Mäuse und Ratten, 3436; Granovit AG, Kaiseraugst, Switzerland). Water was provided *ad libitum*, the day and night cycle included 12 hours of light, from 6 am to 6 pm. The colony was maintained under specific pathogen-free conditions and sentinel animals were confirmed to be free of viral, bacterial, and parasitic pathogens listed in the FELASA recommendations,[37] except for mouse norovirus (MNV) and *Helicobacter*.

The study cohort comprised a total of 109 mice. Among these were 48 NSG mice (31 males, 17 females) that did not receive any treatment. Of these, 10 (6 males, 4 females) were culled at 1-3 months of age, representing animals bred for, but not used in humanization experiments. Thirty-eight (25 males, 13 females) were breeding animals that were culled at 6 months of age, at the end of their breeding career. The second cohort of 61 hu-NSG mice (31 males, 30 females) were subjected to human cell engraftment (inefficiently humanized mice at 3 months of age (n = 22; <15% hCD45^{+} cells in peripheral blood after reconstitution), and efficiently humanized mice at 4-5 months of age (n = 39)). These animals had served as the non-infected control group in an experiment to investigate the effects of Epstein-Barr virus infection on the immune system and were culled at the age of 3-5 months, at termination of the experiment. As part of the above-mentioned experiment on Epstein-Barr virus infection, the animals were injected intraperitoneally with 100 µl PBS at 12 to 14

weeks after irradiation. At the age of 4 months, 4 of these animals, 2 males and 2 females, developed progressive weight loss and signs of unease such as hunched posture, rough coat and reddened skin, and had to be euthanized.

After reconstitution, mice were clinically checked daily for three days, and then three times a week until weaning. A weekly check was performed on mice four weeks and older, including naïve NSG mice.

Human Tissue Engraftment

$CD34^+$ HSC were isolated from fetal livers (Advanced Bioscience Resources, CA, USA) following established protocols.[54] Cells originated from 13 different donors and were frozen in liquid nitrogen prior to their use in the engraftment experiments. At the age of 1-6 days, NSG mice (n=61) were each irradiated with 1Gy (preconditioning), using a "Rad Source 2000" equipped with an X-ray source, and injected intrahepatically 5-7 hours later with $1\text{-}3x10^5$ $CD34^+$ human HSC. After 10-12 weeks, blood was collected via the tail vein and analyzed by FACS. In addition to the above reported morbidity after 4 months, 6% of irradiated and reconstituted hu-NSG pups were lost prior to weaning due to neglect or cannibalism by the mother. It remains unclear if this was connected to irradiation and/or reconstitution.

Ethics Statement

All animal protocols were in accordance with the Swiss Animal Welfare Act, Tierschutzgesetz (TSchG) and were approved by the veterinary office of the canton of Zurich, Switzerland (protocols 148/2011, 209/2014 and 159/17). The studies involving human samples were reviewed and approved by the cantonal ethics committee of Zurich, Switzerland (protocol KEK-StV-Nr.19/08, KEK-ZH-Nr. 2010-0057 and 2019-00837).

187

188 *Macroscopic and Histological Examination*

189 Mice were euthanized by 100% carbon dioxide asphyxiation, followed by
190 exsanguination and creation of a pneumothorax. A full necropsy was conducted on
191 each mouse and a standard selection of organs, hemolymphatic tissues, as well as
192 bones and joints were sampled and fixed in 10% neutral buffered formalin for 48-120
193 hours, then trimmed and routinely embedded in paraffin wax following a predefined
194 blocking pattern. Consecutive sections (3-5 µm) were prepared and routinely stained
195 with hematoxylin and eosin (HE), special stains (when appropriate) or subjected to
196 immunohistochemistry. Examined tissues were adrenal glands, brain, eyes, female
197 genital tract (mammary gland, ovaries, uterus, vagina), gastrointestinal tract
198 (stomach, duodenum, jejunum, ileum, cecum, colon and rectum), Harderian gland,
199 heart, kidneys, liver with gall bladder, lungs, male genital tract (epididymis, prostate,
200 testes, seminal vesicles), pancreas, salivary glands, skeletal muscle (*Musculus*
201 *quadriceps femoris*), skin, spinal cord, tongue, and urinary bladder. Examined
202 hemolymphatic tissues were bone marrow from several locations (see bones), lymph
203 nodes [cervical (one lymph node of the cervical chain: mandibular, accessory
204 mandibular or superficial parotid), mesenteric (colic or jejunal), proper axillary] (in
205 most animals, not all three lymph nodes were successfully sampled as these could
206 not be identified grossly), spleen (1-2 cross sections), and thymus. Since thymus and
207 lymph nodes were difficult to grossly identify especially in NSG mice, tissue in the
208 corresponding area was collected and included in the paraffin block. Bones (sternum,
209 femur and tibia with femorotibial joint, spinal column) as well as the head with nasal
210 and oral cavities and teeth were also collected. After fixation, these were decalcified
211 for 3-5 days in a mild decalcifying solution (RDF, Mild Decalcifier, CellPath, Newtown,
212 UK), followed by paraffin embedding. Special stains were applied when considered

necessary and comprised the Gram, Giemsa, Grocott, and Ziehl-Neelsen stains as well as the periodic acid-Schiff reaction).

Immunohistochemistry

Immunohistochemistry was applied to detect cells of human origin (Ku80$^+$), human and mouse leukocytes (hCD45$^+$, mCD45$^+$), T cells (CD3$^+$, CD4$^+$, CD8$^+$), human and mouse B cells (CD20$^+$ andCD45R-B220$^+$, respectively, monocytes/macrophages (calprotectin$^+$, Iba1$^+$, F4/80$^+$, lysozyme$^+$) and MHC II expression. Antibodies and detection methods are listed in Tables 1 and 2.

Histological Scoring and Histomorphometry

All tissues/organs were examined for histopathological changes which were diagnosed following the International Harmonization of Nomenclature and Diagnostic Criteria (INHAND), Society of Toxicological Pathology (www.toxpath.org/inhand.asp). When appropriate, lesions were graded semi-quantitatively using a score from 1 to 5. Granulomatous inflammation scores were primarily determined by the amount of tissue involvement (1 = minimal [< 1%]; 2 = mild [1–25%]; 3 = moderate [26–50%]; 4 = marked [51–75%]; 5 = severe [76–100%]) as described.[50]

For morphometric evaluation, slides with hemolymphatic tissue sections stained by immunohistochemistry were scanned using a digital slide scanner (NanoZoomer-XR C12000, Hamamatsu Photonics K.K., Iwata City, Japan), the Visiopharm Integrator System (Visiopharm, Hoersholm, Denmark) was used for the subsequent quantitative analysis. The mCD45 and hCD45 positive cell fraction areas and the number of Ku80 (nuclear marker) positive nuclei per high power field were calculated on consecutive sections. The mCD45 positive cell fraction area in hemolymphatic organs

repopulated by human cells was calculated following subtraction of the hCD45 positive area from the total tissue area.

FACS Analysis

FACS served to identify hCD45$^+$, CD3$^+$, CD4$^+$, CD8$^+$, CD19$^+$, NKp46$^+$, CD4/DR$^+$, CD8/DR$^+$ populations and followed previously described protocols.[2] Peripheral blood was collected from hu-NSG mice 3 months after human cell engraftment by tail vein bleeding into heparin-containing tubes (Heparin-Na, Braun). After two rounds of red blood cell lysis, peripheral blood mononuclear cells (PBMCs) were washed with PBS and stained with fluorescence coupled antibodies for 20 minutes at 4 °C. Antibodies are listed in Table 2. Subsequently, cells were fixed in 4% paraformaldehyde diluted in phosphate buffered saline (PBS) for 0 to 24 hours. Data was acquired on the BD FACSCanto II using DIVA software and analysed using FlowJo software Version 10.2. The cells were first gated for singlets, followed by hCD45.

Statistical Analysis

Statistical analysis was conducted using a Statistics Software (SPSS, 23). Correlation between FACS results and abundance of hCD45 positive cells in the lymphoid organ tissue sections was tested using Pearson test. Spearman's correlation analysis was used to study the relationship between granulomatous inflammation and activated T cells. For this analysis, granulomatous inflammation was divided in three categories as 0 = not present; 1 = mild, occurring with low severity and limited distribution; and 2 = severe , occurring with high severity and broad distribution. Statistical significance was evaluated using Mann-Whitney-U-Test and t-test. p values <0.05 were considered statistically significant.

Results

Background lesions and radiation-induced changes

The NSG mouse cohort (n = 48) remained healthy during the examination period and exhibited only a limited selection of histological lesions, with generally low severity (Table 3). The most frequently encountered changes were minimal or mild multifocal alveolar macrophage accumulation with pleural thickening in the lungs; minimal focal tubular basophilia and tubular dilation with epithelial cell hypertrophy in the kidneys; minimal or mild patchy degeneration and dystrophic mineralization of seminiferous tubules in the testes; and minimal to moderate multifocal subcapsular cell hyperplasia in the adrenal glands.[50] The latter occurred with higher frequency in females. Sporadically, minimal or mild focal degenerative changes in the intersternebral and intervertebral joints as well as cortical thickening of the femoral diaphysis were noted. Individual animals exhibited inflammatory processes, such as minimal focal neutrophilic myositis in retro-orbital and masticatory muscles, focal neutrophilic folliculitis in the skin of the muzzle, and a moderate diffuse chronic sialoadenitis. The latter appeared to be the consequence of an obstruction of the main excretory duct by a hair. Also, one mouse showed marked chronic pancreatitis, characterized by diffuse fibrosis, moderate mononuclear cell inflammation and lobular acinar atrophy. Apart from occasional dilation of endometrial glands, the female reproductive tract was free of histopathological changes. Ovaries exhibited numerous follicles at different stages of maturation and corpora lutea. The vagina showed normal cyclic changes consistent with all four phases of the rodent reproductive cycle.

The hu-NSG mice exhibited the same type of background lesions as the NSG mice, and with similar frequency and severity (Table 3). In addition, hu-NSG mice showed

histological changes consistent with exposure to radiation in the early postnatal period, i.e. radiation nephropathy, cataract and impaired retinal development,[4] and ovarian atrophy.[1,6] Radiation nephropathy was characterized as deposition of proteinaceous material and reduced number of capillaries in glomeruli, cortical tubular collapse[40], and was observed in relatively few mice (13% of males, 17% of females) and with minimal severity (Fig. 1). Impaired retinal development was more frequent (more than 70% of animals), and ranged from a thinning of the outer nuclear layer and the outer segment layer, to a lack of distinction between outer and inner nuclear layer, leading to a very thin retina composed of a single row of nuclei (Fig. 2). Changes were more severe in the peripheral portion of the retina. Cataract occurred in fewer mice (Table 3) with low severity and consisted of rupture of the posterior lens capsule with lens fibre fragmentation and focal liquefaction. Almost all female animals exhibited ovarian atrophy of varying degree. In more severe cases, the ovaries were reduced in size and exhibited a marked reduction to complete absence of oocytes, follicles and corpora lutea (Fig. 3). Such animals appeared to be in persistent anestrus, as there was no evidence of estrus cycling in uterus and vagina.

Hemolymphatic tissues

Spleens, lymph node, thymus and bone marrow were compared in both groups of mice, in particular to comparatively assess the murine and human leukocyte component in hu-NSG mice. Based on previous experience of the group, hu-NSG mice were classified as inefficiently humanized (hu-NSG(i) mice), when they exhibited less than 15% hCD45$^+$ cells in the blood (determined by FACS). This applied to 22/61 (40%) of the animals in the present study.

Spleen. In the NSG mice, spleens were generally small, less than 12 x 2 x 1 mm in size, with rare, randomly distributed leukocytes (mCD45$^+$) and no morphological

316 evidence of lymphocytes populating follicles and T cell zones. In 27/48 of the NSG
317 mice, small aggregates of mCD45$^+$ cells were found around one or two arterioles,
318 reminiscent of periarteriolar lymphoid sheaths (PALS; Fig. 4a, b). The aggregates
319 were composed of round to polygonal cells of approximately 15 µm diameter, with
320 scant cytoplasm and a large round to slightly elongated nucleus with finely stippled
321 chromatin and no evident nucleolus. These cells were consistently negative for T cell
322 (CD3), B cell (CD45R-B220) and macrophage (F4/80, calprotectin and lysozyme)
323 markers. The red pulp was mainly populated by erythroid progenitors and some
324 megakaryocytes, representing minimal to moderate extramedullary hematopoiesis
325 (Fig. 4a), and scattered leukocytes; some animals also exhibited minimal
326 hemosiderosis.
327 In all hu-NSG mice, the spleens were substantially larger, approximately 15 x 5 x 2
328 mm on average. Histologically, this was due to the much higher cellularity of the
329 organ secondary to human cell repopulation. While there was no evidence of
330 follicular structures, human cells tended to cluster around splenic arterioles, forming
331 PALS-like structures (Fig. 5) similar to but generally much larger than those formed
332 occasionally by mCD45$^+$ cells in the spleen of NSG mice. In the latter, due to the
333 PALS-like aggregates, the proportion of the area in the spleen covered by mCD45$^+$
334 cells averaged 6% (n = 6; mean = 6.3; SD = ±7.8), but exceeded 10% in individual
335 animals (Fig. 6), whereas murine leukocytes (mCD45$^+$) were extremely rare in hu-
336 NSG mice (Figs. 5b, 6). In contrast, they carried numerous hCD45$^+$ cells (Fig. 5c). In
337 efficiently humanized (hu-NSG(e)) mice, the hCD45-positive cell fraction area was
338 21.0% on average, though the proportion varied considerably between animals
339 (Table 4). In hu-NSG(i)mice, the hCD45 positive cell fraction area had a mean of
340 8.8% (Table 4); however, the difference between the two groups was not significant.
341 The white pulp in hu-NSG mice consisted of B cells (CD20$^+$) and T cells (CD3$^+$) in

equal proportions. The T cells were mostly found in the center of the reconstituted white pulp, in the PALS-like structures around the arteries (Fig. 7a). B cells tended to occupy the periphery of the white pulp but did not arrange in clear follicular structures (Fig. 7b). Immunolabeling for CD4 and CD8 identified mainly $CD4^+$ T cells whereas only random individual cells scattered throughout the parenchyma were $CD8^+$. In all animals, the remaining area (red pulp) was mainly occupied by erythroid progenitor cells, intermingled with megakaryocytes (moderate extramedullary hematopoiesis) and scattered $hCD45^+$ leukocytes with the morphology of lymphocytes; these appeared to be represented by B cells and T cells in equal proportions (Fig. 7).

Lymph nodes. In NSG mice, lymph nodes were generally very small and difficult to identify grossly. However, in the majority of animals, the mesenteric and mandibular lymph nodes were successfully sampled. They were composed predominantly of connective tissue, i.e. the reticular stroma (Fig. 8a). Leukocytes ($mCD45^+$) were present in low numbers, scattered throughout the fibrous scaffold (Fig. 8b). When sampled successfully, axillary and inguinal lymph nodes exhibited the same morphological features.

In hu-NSG mice, lymph nodes were in general larger and therefore easier to identify grossly. Histologically, most lymph nodes were abundantly populated by lymphoid round cells (Fig. 9). They contained only few murine leukocytes ($mCD45^+$; n = 33, mean ± SD = 0.86 ± 1.8 %), and on average less than the lymph nodes of NSG mice (n = 11; 2.8 ± 4.1%) (Fig. 10). Instead, human leukocytes ($hCD45^+$) repopulated the fibrous stroma (n = 33; 42.1 ± 22.4%) (Fig. 9d). In efficiently humanized mice, the hCD45-positive cell fraction area had a mean of 54.1%, whereas in inefficiently humanized mice, the mean was 18.6% (Table 4). In some of the latter animals, no human cells were identified at all; these lymph nodes had morphological features identical to those of the NSG mice. However, also in the efficiently humanized mice,

repopulating hCD45$^+$ cells appeared to distribute randomly across the lymph node, did not aggregate to form appreciable lymphoid follicles or paracortical structures, and did not allow distinction of the cortex and medulla. Accordingly, CD20$^+$ B cells which were present in moderate to high numbers, and CD3$^+$ T cells which were slightly less numerous, were seen randomly distributed throughout the stroma. Overall, the periphery had a higher proportion of B cells (Fig. 9b) while T cells tended to be more numerous in the center (Fig. 9c). Most T cells appeared to be CD4$^+$, whereas CD8$^+$ cells were only present in very small numbers.

Thymus. In NSG mice, the thymus was generally barely visible and composed of hypoplastic lobules that lacked a defined cortex and medulla and often contained cysts, as previously reported (Fig. 11).[7] Again, leukocytes (mCD45$^+$) were rare (Fig. 12).

In hu-NSG mice, the thymus generally appeared slightly larger, with an approximate size of 2 x 1 x 1 mm. Lobules were more cellular and exhibited moderate numbers of lymphoid cells (Fig. 13), but still lacked the typical corticomedullary distinction. Murine leukocytes were rare (Fig.13b): the mCD45 positive cell fraction area had a mean of 0.4% (Fig. 14). Still, mCD45$^+$ cells were sometimes more numerous than in NSG mice, where the area covered by mCD45$^+$ cells did not exceed 0.3% (n = 9; mean ± SD = 0.09 ± 0.1 %) (Fig. 14). Repopulation with hCD45$^+$ leukocytes was variable in hu-NSG mice. In efficiently humanized mice (Fig. 13c), the mean of the hCD45 positive cell fraction area reached 46.1%, whereas it was 16.5% in inefficiently humanized mice (Table 3). The majority of these cells were CD3$^+$. Of this subpopulation, most cells were CD4$^+$ whereas CD8$^+$ cells were only visible in very small numbers. CD20$^+$ cells were barely present.

One 6-month-old female breeding NSG mouse exhibited a white-tan, firm mass of approximately 0.4 cm in diameter in the thoracic cavity. Histologically, it was

composed of dense sheets of large round neoplastic cells which also infiltrated the adjacent adipose tissue (Supplemental Fig. S1). The cells exhibited scant amphophilic cytoplasm and round nuclei with coarsely arranged chromatin. There was moderate anisocytosis and a mitotic rate of 2-4/HPF; a moderate number of apoptotic cells was observed (Supplemental Fig. S2a). The vast majority of cells were found to express CD3 and CD4 (Supplemental Fig. S2b, c), whereas B cells ($CD45R^+$) were seen in low numbers and randomly distributed. This led to the diagnosis of a precursor T cell lymphoblastic lymphoma.[38] It was not possible to determine whether the neoplasia originated from the thymus or the mediastinal lymph nodes. The mouse did not exhibit any additional histopathological changes.

Bone marrow. In NSG mice, the bone marrow (sternal and femoral) generally exhibited a high cellularity, represented by erythroid, $mCD45^+$ myeloid and megakaryocytic hematopoietic precursors (Fig. 15). Mild to moderate hemosiderosis as well as fatty infiltration (femur only) was occasionally seen (Table 2A).

In hu-NSG mice, the morphology of the bone marrow was similar, with high to very high cellularity (Fig. 16). While $mCD45^+$ cells were very rare, making up a significantly lower proportion of area than in the NSG mice (Fig. 16b, 17), $hCD45^+$ cells were the dominant cell population (Figs. 16c). The number of human cells ($Ku80^+$) was significantly higher in efficiently humanized vs inefficiently humanized mice (Table 4).

Granulomatous inflammation in $CD34^+$ hu-NSG mice

Two male and two female hu-NSG mice developed poor health before study completion and were electively euthanized, the females at 28 weeks after HSC transplantation due to severe progressive weight loss, and the males at 30 weeks. Both males were thin and exhibited clinical signs, i.e. hunched posture, rough coat

and reddened skin. All four mice exhibited grossly enlarged lymph nodes and spleen, diffusely pale bone marrow, and a red and white mottled liver. Histological examination revealed extensive granulomatous inflammatory infiltrates in these tissues as well as in the kidneys (Figs. 18-24). There was no evidence of bacterial or fungal organisms within the inflammatory infiltrates, as confirmed by various special stains (Gram, Giemsa, periodic acid-Schiff, Grocott, and Ziehl-Neelsen). [11,53]Granulomatous infiltrates were represented by multifocal to coalescing, partly nodular aggregates of macrophages and epithelioid cells, admixed with numerous lymphocytes and multinucleated giant cells (Figs. 18-24). In the infiltrates, cells were often found to proliferate, which was reflected by the presence of 1-3 mitotic figures per high power field. The vast majority of cells were human leukocytes ($Ku80^+$ (Fig. 19b), $hCD45^+$), with only very few intermingled murine ($mCD45^+$) leukocytes. Macrophages and T cells ($CD3^+$) dominated in the infiltrates which also contained a variable portion of B cells and a few viable neutrophils (Fig. 19c, d). Combined immunohistochemistry for CD4 and CD8 antigens revealed a striking predominance of $CD4^+$ T cells, with only rare CD8 or double-positive cells. In the liver, lesions consisted of lymphohistiocytic or granulomatous infiltrates that were mainly located in periportal areas (Figs. 18, 19a) and were associated with minimal to moderate deposition of fibrous connective tissue as well as scattered hemosiderin-laden macrophages. Bile ducts were often embedded within the inflammatory reaction, but were neither altered nor infiltrated, suggesting that they were not targeted by the inflammatory cells at this stage. Bone marrow changes presented as scattered nodules randomly distributed in the hematopoietic tissue (Fig. 20a) to subtotal replacement of the hematopoietic cell component by, in the majority, MHC II positive cells (Fig. 20b), with concurrent bone marrow necrosis and hemorrhage as well as trabecular bone resorption (data not shown). Affected spleens and lymph nodes

(Figs. 21-24) showed scattered focal infiltrates or severe disruption of the architecture by the inflammatory infiltrates. When affected, kidneys exhibited only mild changes, represented by scattered granulomatous foci randomly distributed throughout the cortical interstitium. In individual cases, pancreas, ovaries, serosae, Harderian glands, nose and/or oral cavity also showed granulomatous infiltrates.

Some animals with the above-described lesions also exhibited inflammatory infiltrates in lungs and skin. In the lungs, these represented peribronchiolar and perivascular aggregates of Ku80-positive cells, which were predominantly T cells and B cells, with fewer macrophages, occasionally containing golden brown pigment, and no evident giant cells. Infiltrates occasionally extended into the bronchiolar and alveolar lumina. In the skin, minimal or mild infiltration of Ku80-positive, predominantly $CD4^+$ and fewer $CD8^+$ T cells and rare B cells was seen at the dermo-epidermal junction, predominantly along the follicular dermo-epidermal junction, associated with vacuolar change and occasional apoptosis in the basal follicular keratinocytes and, to a lesser extent, the basal epidermal keratinocytes.

Granulomatous inflammatory infiltrates were also observed in mice without clinical signs, with lower severity and higher incidence in males (21%; 6/29) than in females (11%; 3/28). Liver, spleen, lymph nodes, bone marrow at different locations (sternum, femur and tibia, vertebrae and frontal bones in the skull) and kidneys were most consistently affected (Table 5). Prevalence and severity of the inflammatory infiltrates was comparable across all engrafted mice, with no obvious differences between the reconstitutions from different donors; however, this could not be specifically addressed due to the low number of mice reconstituted with the same donor.

Comparison of blood and lymphoid tissues

The FACS analysis performed on the peripheral blood of the hu-NSG mice revealed a large variability in the proportion of human leukocytes (hCD45$^+$), ranging from 0.14% to 66.5% (Figs. 25, 26). As mentioned above, mice with more than 15% hCD45$^+$ cells in the blood were considered as efficiently humanized (Figs. 25, 27), and below this threshold as inefficiently humanized (Figs. 26, 28).

Immunohistochemistry against hCD45 was performed on the lymphoid organs of a random selection of efficiently and inefficiently humanized mice (each n = 8) to correlate with the FACS data. As expected, this grouping of mice matched to some extent with the degree of repopulation of the hemolymphatic organs, as overall the percentage of human cells was significantly higher in lymph nodes, thymus and bone marrow of the efficiently compared to the inefficently humanized mice (Table 4). Interestingly, there was no substantial difference in the spleen. This may be due to the overall low relative extent of repopulation of this organ, which still contained a significant proportion of murine hematopoietic cells; even in efficiently humanized mice, the mean percentage area covered by human leukocytes (hCD45$^+$) was 21.0%, whereas it was 46.1% and 54.1% in thymus and lymph nodes respectively (Table 3). However, looking at repopulation levels in the different organs of individual animals it became obvious that there was substantial variation. The bone marrow was specifically analyzed because it can be expected to be most relevant for the production of cells that later appear in the blood stream. However, a mouse classified as inefficiently humanized could have a proportion of human cells in the bone marrow that was as high as that seen in efficiently humanized mice (Figs. 26, 28).

The FACS results of animals with evidence of granulomatous inflammation (n = 13) were compared with those of mice without such lesions (n = 48). Interestingly, animals with granulomatous inflammation were found to have significantly lower proportions of human leukocytes (Table 6). In the latter, the human leukocyte

population contained significantly lower total lymphocyte proportions and B cells, but significantly higher proportions of T cells and monocytes. There were also significantly more activated T cells, activated T helper cells and activated cytotoxic T cells (Table 6) (correlation coefficient of 0.630 for $CD4DR^+$ and of 0.661 for $CD8DR^+$ cells, Spearman's correlation analysis).

Discussion

Data illustrating the spectrum of spontaneous and experimentally induced diseases in humanized mice are very limited, and the situation is similar for the recipient NSG immunodeficient mice. Besides, detailed characterization of the morphological aspects of repopulation at tissue level is highly desirable to allow accurate correlation with the engraftment features obtained via FACS analysis. This study aimed to characterise the morphological phenotype of NSG mice and their humanized counterpart, the $CD34^+$ hu-NSG murine model, and to gather data on the most common background lesions in both types of mice. In addition, a comparative quantitative assessment was undertaken in the attempt to relate levels of human repopulation in the hemolymphatic organs of hu-NSG mice to FACS results obtained from the peripheral blood, as the latter is commonly used as a tool to determine the extent of humanization.

Full histological examination of a cohort of 48 NSG mice aged 3 to 6 months revealed a limited spectrum of background lesions, occurring with low severity. Salient changes were observed in lungs, kidneys, testes and adrenal glands and were all among those commonly encountered in other strains.[13,17,44] In addition, there was a very low prevalence of incidental inflammatory changes, without evidence of infectious conditions. This can likely be ascribed to housing of the mice under specific

pathogen free conditions as in general NSG mice are prone to infections because their immune system is compromised.[16]

Since the present study focused on young animals, it cannot provide data on potential spontaneous neoplastic processes that might develop with age.[47] Interestingly though, lymphoma was found in the thoracic cavity of a 6-month-old non-irradiated female NSG mouse, which could have originated from the thymus or the mediastinal lymph nodes. The tumor was predominantly composed of $CD3^+$, $CD4^+$ T cells and further characterized as a T cell lymphoblastic lymphoma. Hematopoietic neoplasms are reported to occur with low prevalence in NSG mice, in subjects older than 1 year,[16,47] due to the inactivation of IL-2Rγ, which plays an important role in the signalling pathways for B and T cell growth.[26] In the present case, it could be a spontaneous event that might have compensated for IL-2Rγ deficiency, and led to full manifestation of the NOD-scid background phenotype, which has been reported to frequently develop lymphoma.[41] Lymphoma, especially thymic lymphoma might also occur secondarily to irradiation, which is used to deplete mouse hematopoetic cells prior to human cell engraftment, or insertional mutagenesis resulting from gene editing therapeutic products. Hence, it is crucial to report on the occurrence of such tumors in untreated NSG mice at an age when they are used in transplantation experiments, to build an accurate historical database.

All NSG mice in the present study showed poorly developed lymphoid organs, lacking the typical lymphoid tissue architecture. This has previously been reported as a feature in the lymphoid organs of several immunodeficient murine lines, including NSG mice, whose genetic manipulation leads to severe impairment of immune functions.[7,47,49,52] However, we observed small or moderately sized periarteriolar clusters of $mCD45^+$ cells in the spleen of numerous NSG mice, a feature that has to our knowledge not been reported yet. Cells in these clusters did not express more

549 specific lymphocyte or macrophage markers, so further work is needed to assess
550 their exact nature and whether they represent early lymphoid precursors, dendritic or
551 myeloid subsets. According to the experience of the authors, these aggregates can
552 complicate the histologic interpretation of NSG mice engrafted with human
553 hematopoietic cells or administered cell-based therapy products, which might have
554 morphological features similar to these native cells in HE-stained sections. Another
555 interesting observation was that, like the bone marrow in *scid* and other
556 immunodeficient mouse lines, the bone marrow of NSG mice did not show major
557 histological abnormalities in the hematopoetic cell component.[14]
558 The comprehensive histological screening of hu-NSG mice, i.e. NSG mice engrafted
559 with human $CD34^+$ HSC, revealed a spectrum of spontaneous lesions similar to that
560 observed in naïve NSG mice. However, the mice additionally exhibited changes that
561 can be ascribed to either the preconditioning irradiation and/or the engraftment of
562 human hematopoietic cells.
563 Among the lesions potentially related to perinatal total body irradiation, to which the
564 *scid* mutation of NSG mice renders them particularly sensitive,[5] were nephropathy,
565 ovarian atrophy and ocular changes. All three are well-known complications of
566 radiation exposure in humans.[3,12] Radiation nephropathy has also been described in
567 different preclinical species including mice.[12] In both humans and laboratory animals
568 it represents a late onset, adverse event following external beam irradiation or
569 radionuclide therapy, characterized by concurrent injury to glomerular and tubular
570 compartments.[12,40] In the present study it was observed with low frequency and
571 severity, which suggests an early stage of the disease in the still-young hu-NSG
572 mice. At this early stage, radiation-induced lesions can be hard to differentiate from
573 tubular basophilia and the early changes that can occur in the context of chronic

574 progressive nephropathy, a common degenerative spontaneous disease in the
575 kidneys of mice and rats.[17]
576 So far, both ovarian atrophy and retinal changes have only been sporadically
577 reported as radiation-induced alterations in animal models, and the present report is
578 the first of such lesions in hu-NSG mice undergoing perinatal preconditioning.
579 Interestingly, both types of changes occurred with high prevalence and severity,
580 indicating a high sensitivity of ovaries and retina of these mice to irradiation. It is
581 known that the germline cells in the ovary are highly susceptible to radiation damage
582 and that accelerated reproductive aging can occur when the follicle pool, which is
583 finite and non-renewable, is damaged due to irradiation.[1] From the present findings it
584 could be speculated that radiation-induced damage of the female germ cells at an
585 early prepubertal stage might cause loss of ovarian reserve, which then manifests as
586 atrophy of the gonads and lack of cyclical changes in uterus and vagina.
587 Interestingly, there were no substantial microscopic changes in the testes of hu-NSG
588 mice, suggesting that the irradiation procedure did not affect the male germline. This
589 difference might be due to different radiation exposure or reduced sensitivity of the
590 male gonadal tissues in the postnatal period, as previously reported.[15]
591 Radiation retinopathy in humans encompasses a number of retinal changes following
592 exposure to radiation from any source, typically external beam radiation exposure in
593 patients affected by tumors of the nasopharynx, sinus or orbita.[3] In animal models,
594 complications of ocular radiation have been reported as rare, most frequently
595 manifesting as cataracts, which also occurred in this study with low prevalence and
596 low severity.[43] The retinal lesions observed in our mouse cohort suggest a perinatal
597 arrest of the retinal development, allowing only the neuroblastic layer and the
598 ganglion cell layer to be identified.[59] To our knowledge, these retinal lesions have not
599 been previously reported in mice that have undergone total body irradiation.

Extensive photoreceptor loss and impaired retinal development in the hu-NSG mice might therefore be linked to radiation exposure in the perinatal period, when cell proliferation is still ongoing in the retina as part of the postnatal development process. Nonetheless, a more thorough investigation of the retinal changes was beyond the scope of the present study, as it would require dedicated long-term studies with multiple endpoints and multiple radiation quantities. Notably though, researchers should be aware of potential impaired vision resulting from the retinal lesions. Impaired retinal development affects predominantly the outer layers, hence resembling outer retinal atrophy, from which it needs to be differentiated. The latter is characterized by loss of photoreceptors and is caused by a number of factors, including aging and phototoxicity.[42]

The changes that can be ascribed to the engraftment of human hematopoetic cells are represented by granulomatous inflammatory infiltrates of almost exclusively human origin that were found in multiple organs of around 20% of hu-NSG mice. The absence of microorganisms and foreign material and the dominance of macrophages and $CD4^+$ T cells suggest either an uncontrolled proliferation of activated human immune cells and/or an underlying human-anti-mouse immunopathological process. Granulomatous infiltrates containing hemosiderin-laden macrophages are reminiscent of post-transplant hemophagocytic lymphohistiocytosis (HLH), an hyperinflammatory condition driven by hypercytokinemia and triggered, for example, by transplantation of HSC.[46] The disease has been reproduced in perforin-deficient mice infected with lymphocytic choriomeningitis virus[27] and in humanized mice following experimental infection with EBV.[48] More recently, it has also been described in NSG-SGM3 mice without human thymus, engrafted with human $CD34^+$ fetal liver cells.[63] The infiltrates in these mice were similar to the lymphohistiocytic infiltrates observed in hu-NSG mice in our study and were not present in NSG mice. However,

626 in general, the inflammatory infiltrates in CD34+ HSC humanized NSG mice as in our
627 study exhibit only occasional hemosiderin-laden macrophages and, in the lungs,
628 have a predominantly lymphocytic rather than histiocytic/granulomatous character. In
629 the liver, inflammatory foci were predominantly present in portal areas, but seemed
630 not to target the biliary ducts; the latter is a striking feature of GvHD in humans. To
631 date, a number of studies have reported multiorgan infiltrates of lymphocytes and
632 macrophages, occasionally with epithelioid macrophages and giant cells, as a
633 manifestation of GvHD in humanized mice,[11,18,28,34,53] and report GvHD as a major
634 cause of morbidity in studies employing humanized mice.[21,28] Considering that
635 Yoshihara and co-authors consider lymphohistiocytic infiltrates with a prominent
636 hemophagocytic component as indicative of HLH rather than GvHD it is also possible
637 that both conditions manifest concurrently in the same model. This seems likely in
638 our murine model, where the inflammatory processes observed in the skin of a few
639 mice, i.e. an interface dermatitis with vacuolation and apoptosis of keratinocytes in
640 the basal layer of hair follicles, closely resemble the typical manifestation of chronic
641 GvHD in human patients, while the multisystemic granulomatous infiltration would
642 rather suggest an uncontrolled proliferation of human macrophages driven by an
643 excess in cytokines, as in HLH.[27,46] In the absence of additional evidence pointing
644 toward one entity or the other, we feel that other methodological approaches, such as
645 T cell receptor repertoire analysis and quantification of plasma and tissue cytokine
646 levels are needed to provide more insight into the exact nature and pathogenesis of
647 these inflammatory lesions.[11,21,51]
648 Since mice affected by granulomatous inflammation do not reach the experimental
649 end-point they are often excluded from the analysis. Thus, the frequency of the
650 respective pathological changes, whose underlying cause is ascribed to GvHD or
651 HLH, is rarely reported.[3] In the present study, thirteen mice showed weight reduction

or clinical signs and all but one of them exhibited granulomatous inflammation, with more males found to be affected (21%) than females (11%). These data indicate that monitoring of weight loss and clinical signs can identify the majority of mice with these specific pathological changes. Still, some mice with only few and mild lesions that can only be detected by histological examination may not be identified based on clinical signs, yet these may show an aberrant immunological response of the engrafted human cells in different types of experiments. It is important to highlight though that the prevalence and features of granulomatous inflammation reported here might solely apply to the model employed in our study, as there is growing evidence that the incidence and severity of inflammatory lesions varies extensively across experiments depending on the source, number and manipulation of human donor cells employed and the features of the recipient host system (e.g. strain susceptibility, environmental features and preconditioning protocols involving irradiation or chemotherapy).[20,36]

In the present study, the *in situ* detection of human and murine cells in the hemolymphatic tissues provided information on the extent and distribution of homing of graft and host leukocytes after humanization with $CD34^+$ HSC. We observed that the mouse component ($mCD45^+$ cells) generally decreased with humanization of the animal, even though the difference was not statistically significant. This phenomenon cannot be explained without further studies employing larger numbers of animals. It could simply be a consequence of irradiation; alternatively, it is possible that the introduction of human cells leads to a reduced proliferation of the murine leukocytes. Both FACS data and the image analysis of tissue sections of hemolymphatic organs suggested that the extent of $hCD45^+$ repopulation was highly variable among the engrafted animals. The reason for this is not clear, but pre-treatment, injection route, and source of HSCs will inevitably have an impact on the inter- and intra-

678 experimental variability of engraftment. This makes comparisons across different
679 models difficult, even when experimental conditions vary only slightly. Human cells
680 showed a variable distribution in the different organs. In the spleen, hCD45$^+$ cells
681 formed aggregates reminiscent of the white pulp of immunocompetent mice, despite
682 the absence of discernible PALS and lymphoid follicle organisation. The thymus of
683 hu-NSG mice was variably repopulated by human T cells, providing further evidence
684 of some functional homing of the lymphocytes; however, the typical architecture was
685 not observed. In the lymph nodes, however, there was no evidence of a cell type-
686 specific arrangement. It has previously been suggested that the genetic background
687 of the mice is responsible for the lack of the typical architecture in the lymphoid
688 organs, as γ_c deficiency compromises IL-7-dependent lymphoid tissue inducer cell
689 development.[33] The architecture is crucial for the proper functionality of the immune
690 system,[39] and it has been suggested that the poorly organized lymphoid organs are a
691 limiting factor in the humoral immune response of humanized mice.[61] Repopulation of
692 the bone marrow seems to be less complicated; in - bone marrows free of
693 inflammatory lesions, all cell types appeared to home effectively.
694 The present study also investigated the correlation between the pattern and extent of
695 reconstitution in the lymphoid organs by human leukocytes and the results of the
696 FACS analysis on peripheral blood. The FACS analysis revealed a high variability in
697 reconstitution between different animals, and similarly the actual distribution of
698 hCD45$^+$ in the lymphoid organs of an individual can be quite variable. Upon pairing
699 the obtained FACS data of the reconstitution 3 to 6 months after human HSC
700 injection with the morphological analysis of the lymphoid organs it became evident
701 that a high reconstitution based on analysis of blood does not necessarily correlate
702 with a high repopulation at the tissue level. In the efficiently humanized mice there
703 was no significant correlation between the level of circulating hCD45$^+$ cells and the

number of hCD45$^+$ cells in the organs, whereas a significant correlation was seen in the inefficiently humanized animals. This significance may be due to the low hCD45$^+$ cell levels in all the compartments and thus a lower variability.

In the animals affected by granulomatous infiltrates the proportion of human leukocytes and lymphocytes in the blood were significantly lower compared to mice that did not exhibit evidence of such inflammatory changes. This might result from migration of human leukocytes from the blood stream to the sites of injury, similarly to what occurs in infections and sepsis,[55] and by compromised hematopoietic function due to granulomatous lesions in the bone marrow, as was visible in the histological evaluation of some of the animals. However, compared to the cohort not affected by granulomatous inflammation, those affected by this process had a significantly higher proportion of T cells in the blood including higher numbers of activated T cells, activated T helper cells and activated cytotoxic T cells. The increased numbers of T cells fit with the central role of effector graft donor T cells in driving these post-transplant pathological processes.[10,36] Moreover, the granulomatous lesions in the bone marrow of affected animals were dominated by MHC II-positive cells, and also activated T cells are known to express this surface antigen.[30] This hypothesis is supported by a study that shows an increase in the proportion and extent of fluctuation of CD3$^+$CD4$^+$CD8β$^+$ T cells.[10]

Identification of an increase in T cells, primarily activated helper T cells in the FACS data might help to spot individual mice affected by subclinical inflammatory lesions, which could then be confirmed via the histological examination of typically affected organs such as the bone marrow, liver and kidneys.

Acknowledgements

The authors wish to thank the technical staff of the Histology Laboratory, Laboratory for Animal Model Pathology, Institute of Veterinary Pathology, Vetsuisse Faculty, University of Zurich, for excellent technical support.

CM is supported by Cancer Research Switzerland (KFS-4091-02-2017), KFSP-Precision^{MS} of the University of Zurich, the Vontobel Foundation, the Baugarten Foundation, the Sobek Foundation, the Swiss Vaccine Research Institute, Roche, ReiThera and the Swiss National Science Foundation (310030B_182827 and CRSII5_180323).

References

1 Adriaens I, Smitz J, Jacquet P. The current knowledge on radiosensitivity of ovarian follicle development stages. *Hum Reprod Update*. 2009;3;359–377.

2 Antsiferova O, Müller A, Rämer PC, et al. Adoptive transfer of EBV specific CD8+ T cell clones can transiently control EBV infection in humanized mice. *PLoS Pathog*. 2014;8;e1004333.

3 Bawankar P, Barman M, Bhattacharjee H, Soibam R, Paulbuddhe V. Radiation retinopathy after external beam irradiation for nasopharyngeal carcinoma: A case report and review of the literature. *Practical Radiation Oncology*. 2018;6;366–368.

4 Borges HL, Chao C, Xu Y, Linden R, Wang JYJ. Radiation-induced apoptosis in developing mouse retina exhibits dose-dependent requirement for ATM phosphorylation of p53. *Cell Death and Differentiation*. 2004;5;494.

5 Bosma MJ, Carroll AM. The SCID mouse mutant: definition, characterization, and potential uses. *Annu Rev Immunol*. 1991;323–350.

6 Braga-Tanaka I, Tanaka S, Kohda A, et al. Experimental studies on the biological effects of chronic low dose-rate radiation exposure in mice: overview of the studies at the Institute for Environmental Sciences. *Int J Radiat Biol*. 2018;5;423–433.

7 Brehm MA, Cuthbert A, Yang C, et al. Parameters for establishing humanized mouse models to study human immunity: analysis of human hematopoietic stem cell engraftment in three immunodeficient strains of mice bearing the IL2rgamma(null) mutation. *Clin Immunol*. 2010;1;84–98.

8 Brehm MA, Shultz LD, Luban J, Greiner DL. Overcoming current limitations in humanized mouse research. *J Infect Dis*. 2013;S125-30.

9 Brehm MA, Wiles MV, Greiner DL, Shultz LD. Generation of improved humanized mouse models for human infectious diseases. *J Immunol Methods*. 2014;3–17.

10 Brinkman RR, Gasparetto M, Lee S-JJ, et al. High-content flow cytometry and temporal data analysis for defining a cellular signature of graft-versus-host disease. *Biol Blood Marrow Transplant*. 2007;6;691–700.

11 Chandra S, Cristofori P, Fonck C, O'Neill CA. Ex Vivo Gene Therapy: Graft-versus-host Disease (GVHD) in NSG™ (NOD.Cg-Prkdcscid Il2rgtm1Wjl/SzJ) Mice Transplanted with CD34+ Human Hematopoietic Stem Cells. *Toxicol Pathol*. 2019;192623319844484.

12 Cohen EP, Robbins MEC. Radiation nephropathy. *Semin Nephrol*. 2003;5;486–499.

13 Creasy D, Bube A, Rijk E de, et al. Proliferative and nonproliferative lesions of the rat and mouse male reproductive system. *Toxicol Pathol*. 2012;6 Suppl;40S-121S.

14 Custer RP, Bosma GC, Bosma MJ. Severe combined immunodeficiency (SCID) in the mouse. Pathology, reconstitution, neoplasms. *Am J Pathol*. 1985;3;464–477.

15 Forand A, Messiaen S, Habert R, Bernardino-Sgherri J. Exposure of the mouse perinatal testis to radiation leads to hypospermia at sexual maturity. *Reproduction*. 2009;3;487–495.

16 Foreman O, Kavirayani AM, Griffey SM, Reader R, Shultz LD. Opportunistic bacterial infections in breeding colonies of the NSG mouse strain. *Vet Pathol*. 2011;2;495–499.

17 Frazier KS, Seely JC, Hard GC, et al. Proliferative and nonproliferative lesions of the rat and mouse urinary system. *Toxicol Pathol*. 2012;4 Suppl;14S-86S.

18 Fujii H, Luo Z-J, Kim HJ, et al. Humanized Chronic Graft-versus-Host Disease in NOD-SCID il2rγ-/- (NSG) Mice with G-CSF-Mobilized Peripheral Blood Mononuclear Cells following Cyclophosphamide and Total Body Irradiation. *PLoS ONE*. 2015;7;e0133216.

19 Gille C, Orlikowsky TW, Spring B, et al. Monocytes derived from humanized neonatal NOD/SCID/IL2Rγ(null) mice are phenotypically immature and exhibit functional impairments. *Hum Immunol*. 2012;4;346–354.

20 Gorin N-C, Piantadosi S, Stull M, Bonte H, Wingard JR, Civin C. Increased risk of lethal graft-versus-host disease-like syndrome after transplantation into NOD/SCID mice of human mobilized peripheral blood stem cells, as compared to bone marrow or cord blood. *J Hematother Stem Cell Res*. 2002;2;277–292.

21 Greenblatt MB, Vrbanac V, Vbranac V, et al. Graft versus host disease in the bone marrow, liver and thymus humanized mouse model. *PLoS ONE*. 2012;9;e44664.

22 Greiner DL, Hesselton RA, Shultz LD. SCID Mouse models of human stem cell engraftment. *Stem Cells*. 1998;3;166–177.

23 Ishikawa F, Yasukawa M, Lyons B, et al. Development of functional human blood and immune systems in NOD/SCID/IL2 receptor γ chainnull mice. *Blood*. 2005;5;1565–1573.

24 Ito M, Hiramatsu H, Kobayashi K, et al. NOD/SCID/gamma©(null) mouse: an excellent recipient mouse model for engraftment of human cells. *Blood*. 2002;9;3175–3182.

25 Ito M, Kobayashi K, Nakahata T. NOD/Shi-scid IL2rgamma(null) (NOG) mice more appropriate for humanized mouse models. *Curr Top Microbiol Immunol*. 2008;53–76.

26 Ito R, Takahashi T, Katano I, Ito M. Current advances in humanized mouse models. *Cell Mol Immunol*. 2012;3;208–214.

27 Jordan MB, Hildeman D, Kappler J, Marrack P. An animal model of hemophagocytic lymphohistiocytosis (HLH): CD8+ T cells and interferon gamma are essential for the disorder. *Blood*. 2004;3;735–743.

28 King MA, Covassin L, Brehm MA, et al. Human peripheral blood leucocyte non-obese diabetic-severe combined immunodeficiency interleukin-2 receptor gamma chain gene mouse model of xenogeneic graft-versus-host-like disease and the role of host major histocompatibility complex. *Clin Exp Immunol*. 2009;1;104–118.

29 Koboziev I, Jones-Hall Y, Valentine JF, Webb CR, Furr KL, Grisham MB. Use of Humanized Mice to Study the Pathogenesis of Autoimmune and Inflammatory Diseases. *Inflamm Bowel Dis*. 2015;7;1652–1673.

30 Lal G, Shaila MS, Nayak R. Activated mouse T-cells synthesize MHC class II, process, and present morbillivirus nucleocapsid protein to primed T-cells. *Cell Immunol*. 2005;2;133–145.

31 Lan P, Tonomura N, Shimizu A, Wang S, Yang Y-G. Reconstitution of a functional human immune system in immunodeficient mice through combined human fetal thymus/liver and CD34+ cell transplantation. *Blood*. 2006;2;487–492.

32 Lang J, Kelly M, Freed BM, et al. Studies of lymphocyte reconstitution in a humanized mouse model reveal a requirement of T cells for human B cell maturation. *J Immunol*. 2013;5;2090–2101.

33 Li Y, Masse-Ranson G, Garcia Z, et al. A human immune system mouse model with robust lymph node development. *Nat Methods*. 2018;8;623–630.

34 Lockridge JL, Zhou Y, Becker YA, et al. Mice engrafted with human fetal thymic tissue and hematopoietic stem cells develop pathology resembling chronic graft-versus-host disease. *Biol Blood Marrow Transplant*. 2013;9;1310–1322.

35 Lysenko V, McHugh D, Behrmann L, et al. Humanised mouse models for haematopoiesis and infectious diseases. *Swiss Med Wkly*. 2017;w14516.

36 MacDonald KPA, Hill GR, Blazar BR. Chronic graft-versus-host disease: biological insights from preclinical and clinical studies. *Blood*. 2017;1;13–21.

37 Mähler Convenor M, Berard M, Feinstein R, et al. FELASA recommendations for the health monitoring of mouse, rat, hamster, guinea pig and rabbit colonies in breeding and experimental units. *Lab Anim*. 2014;3;178–192.

38 Morse HC, Anver MR, Fredrickson TN, et al. Bethesda proposals for classification of lymphoid neoplasms in mice. *Blood*. 2002;1;246–258.

39 Pearson T, Shultz LD, Miller D, et al. Non-obese diabetic-recombination activating gene-1 (NOD-Rag1 null) interleukin (IL)-2 receptor common gamma

chain (IL2r gamma null) null mice: a radioresistant model for human lymphohaematopoietic engraftment. *Clin Exp Immunol*. 2008;2;270–284.

40 Pellegrini G, Siwowska K, Haller S, et al. A short-term biological indicator for long-term kidney damage after radionuclide therapy in mice. *Pharmaceuticals (Basel)*. 2017;2.

41 Prochazka M, Gaskins HR, Shultz LD, Leiter EH. The nonobese diabetic scid mouse: model for spontaneous thymomagenesis associated with immunodeficiency. *Proc Natl Acad Sci U S A*. 1992;8;3290–3294.

42 Ramos MF, Baker J, Atzpodien E-A, et al. Nonproliferative and proliferative lesions of the rat and mouse special sense organs (ocular [eye and glands], olfactory and otic). *J Toxicol Pathol*. 2018;3 Suppl;97S-214S.

43 Ramos MS, Echegaray JJ, Kuhn-Asif Dacvo S, et al. Animal models of radiation retinopathy - From teletherapy to brachytherapy. *Exp Eye Res*. 2019.

44 Renne R, Brix A, Harkema J, et al. Proliferative and nonproliferative lesions of the rat and mouse respiratory tract. *Toxicol Pathol*. 2009;7 Suppl;5S-73S.

45 Rongvaux A, Willinger T, Martinek J, et al. Development and function of human innate immune cells in a humanized mouse model. *Nat Biotechnol*. 2014;4;364–372.

46 Sandler RD, Carter S, Kaur H, Francis S, Tattersall RS, Snowden JA. Haemophagocytic lymphohistiocytosis (HLH) following allogeneic haematopoietic stem cell transplantation (HSCT)-time to reappraise with modern diagnostic and treatment strategies? *Bone Marrow Transplant*. 2020;2;307–316.

47 Santagostino SF, Arbona RJR, Nashat MA, White JR, Monette S. Pathology of aging in NOD scid gamma female mice. *Vet Pathol*. 2017;5;855–869.

48 Sato K, Misawa N, Nie C, et al. A novel animal model of Epstein-Barr virus-associated hemophagocytic lymphohistiocytosis in humanized mice. *Blood*. 2011;21;5663–5673.

49 Seymour R, Sundberg JP, Hogenesch H. Abnormal lymphoid organ development in immunodeficient mutant mice. *Vet Pathol*. 2006;4;401–423.

50 Shackelford C, Long G, Wolf J, Okerberg C, Herbert R. Qualitative and quantitative analysis of nonneoplastic lesions in toxicology studies. *Toxicol Pathol*. 2002;1;93–96.

51 Shultz LD, Brehm MA, Garcia-Martinez JV, Greiner DL. Humanized mice for immune system investigation: progress, promise and challenges. *Nat Rev Immunol*. 2012;11;786–798.

52 Shultz LD, Lyons BL, Burzenski LM, et al. Human lymphoid and myeloid cell development in NOD/LtSz-scid IL2R null mice engrafted with mobilized human hemopoietic stem cells. *J Immunol*. 2005;10;6477–6489.

53 Sonntag K, Eckert F, Welker C, et al. Chronic graft-versus-host-disease in CD34(+)-humanized NSG mice is associated with human susceptibility HLA haplotypes for autoimmune disease. *J Autoimmun*. 2015;55–66.

54 Strowig T, Chijioke O, Carrega P, et al. Human NK cells of mice with reconstituted human immune system components require preactivation to acquire functional competence. *Blood*. 2010;20;4158–4167.

55 Tanaka J, Sato T, Jones RT, Trump BF, Cowley RA. The pathophysiology of septic shock: responses to different doses of live Escherichia coli injection in rats. *Adv Shock Res*. 1983;101–114.

56 Tanaka S, Saito Y, Kunisawa J, et al. Development of mature and functional human myeloid subsets in hematopoietic stem cell-engrafted NOD/SCID/IL2rγKO mice. *J Immunol*. 2012;12;6145–6155.

57 Theocharides APA, Rongvaux A, Fritsch K, Flavell RA, Manz MG. Humanized hemato-lymphoid system mice. *Haematologica*. 2016;1;5–19.

58 Unanue ER. Antigen presentation in the autoimmune diabetes of the NOD mouse. *Annu Rev Immunol*. 2014;579–608.

59 van Cruchten S, Vrolyk V, Perron Lepage M-F, et al. Pre- and postnatal development of the eye: a species comparison. *Birth Defects Res*. 2017;19;1540–1567.

60 Vuyyuru R, Patton J, Manser T. Human immune system mice: current potential and limitations for translational research on human antibody responses. *Immunol Res*. 2011;2-3;257–266.

61 Walsh NC, Kenney LL, Jangalwe S, et al. Humanized mouse models of clinical disease. *Annu Rev Pathol*. 2017;187–215.

62 Yahata T, Ando K, Nakamura Y, et al. Functional human T lymphocyte development from cord blood CD34+ cells in nonobese diabetic/Shi-scid, IL-2 receptor null mice. *J Immunol*. 2002;1;204–209.

63 Yoshihara S, Li Y, Xia J, Danzl N, Sykes M, Yang Y-G. Posttransplant hemophagocytic lymphohistiocytosis driven by myeloid cytokines and vicious cycles of T-cell and macrophage activation in humanized mice. *Front Immunol*. 2019;186.

64 Zhang B, Duan Z, Zhao Y. Mouse models with human immunity and their application in biomedical research. *J Cell Mol Med*. 2008;6;1043–1058.

927 **Figure legends**

928 **Figures 1-3**. Radiation exposure (one-time irradiation with 1Gy at the age of 1-6
929 days), hu-NSG mouse. Hematoxylin and eosin. **Figure 1**. Kidney. Radiation
930 nephropathy. Cortical tubules are collapsed (arrows in main image and top inset).
931 Inset bottom: There is deposition of proteinaceous material and reduced number of
932 capillaries in a glomerulus (arrowhead). **Figure 2**. Eye. Most structures of the retina
933 cannot be identified. There appears to be an irregular ganglion cell layer (GCL) and a
934 defined neuroblastic layer (NBL) of up to six cell layers. **Figure 3**. Ovary. The ovary is
935 small and devoid of follicles and corpora lutea.
936
937 **Figures 4-7**. Spleen. **Figure 4**. NSG mouse. **a**. There are no distinct white pulp
938 structures. Occasional aggregates of round cells form structures reminiscent of
939 periarteriolar lymphoid sheaths (PALS) (arrows). The red pulp is cell-rich, mainly due
940 to extramedullary hematopoiesis. Inset: PALS-like structure (arrowhead: artery).
941 Hematoxylin and eosin (HE). **b**. The PALS-like structures are comprised of $mCD45^+$
942 cells that aggregate around a splenic arteriole (arrowhead). Numerous $mCD45^+$ cells
943 are also randomly distributed in the red pulp. Immunohistochemistry, hemalaun
944 counterstain. **Figure 5**. hu-NSG mouse. **a**. The white pulp is prominent, with large
945 aggregates of lymphoid cells clustering around arterioles (arrowhead), consistent with
946 PALS. The red pulp is cell-rich, with abundant extramedullary hematopoiesis. HE. **b**.
947 Murine leukocytes ($mCD45^+$) are rare (arrowheads). Inset: Higher magnification of
948 $mCD45^+$ cells (arrowheads). Immunohistochemistry, hemalaun counterstain. **c**.
949 Human leukocytes ($hCD45^+$) form the PALS-like aggregates and are also distributed
950 in moderate number throughout the red pulp (hCD45-positive cell fraction area of
951 13.4%). Immunohistochemistry, hemalaun counterstain. **Figure 6**. Boxplot presenting
952 the area in the spleen of NSG and hu-NSG mice covered by $mCD45^+$ cells (mCD45

positive cell fraction area in %). There is a trend toward a lower percentage of mCD45$^+$ cells in hu-NSG mice, however, the difference is not statistically significant ($p = 0.148$). **Figure 7**. hu-NSG mouse. **a**. The PALS-like structures around the arteries are mainly comprised of T cells (CD3$^+$). **b**. B cells (CD20$^+$) arrange around the PALS-like structures, without forming clear follicles. Immunohistochemistry, hemalaun counterstain.

Figures 8-10. Lymph nodes. **Figure 8**. Mesenteric lymph node, NSG mouse. **a**. The lymph node is very small. The inset shows that it is mainly represented by a meshwork of fibrous tissue (reticular stroma), with low numbers of embedded leukocytes (arrowheads). Hematoxylin and eosin (HE) . **b**. The lymph node contains only few mCD45$^+$ leukocytes. Immunohistochemistry, hemalaun counterstain. **Figure 9**. Mesenteric lymph node, hu-NSG mouse (well repopulated; hCD45-positive cell fraction area of 43.2%). **a**. The lymph node exhibits high cellularity, although no clear follicular and paracortical structures are identified. HE. **b, c**. The repopulating cells are B cells (b, CD20$^+$) and T cells (c, CD3$^+$) that seem to cluster to some extent but do not form follicles or T cell zones. **d**. Almost all cells are hCD45-positive. Immunohistochemistry, hemalaun counterstain. **Figure 10**. Boxplot presenting the area in the lymph nodes of NSG and hu-NSG mice covered by mCD45$^+$ cells (mCD45 positive cell fraction area in %). There is a trend toward a lower percentage of mCD45$^+$ cells in hu-NSG mice, however, this is not statistically significant ($p = 0.059$).

Figures 11-14. Thymus. **Figures 11, 12**. NSG mouse. **Figure 11**. Hypoplastic thymus without defined cortex and medulla, devoid of lymphocytes and with a large cyst (*). Hematoxylin and eosin (HE). **Figure 12**. Leukocytes (mCD45$^+$) are found in

low numbers and randomly distributed (arrowhead). Immunohistochemistry, hemalaun counterstain. **Figure 13**. hu-NSG mouse. **a**. Cortex and medulla cannot be identified, but there is a moderate cellularity with numerous disseminated lymphoid cells. HE. **b**. Murine leukocytes (mCD45$^+$) are disseminated in low numbers. **c**. The vast majority of the lymphoid cells are hCD45$^+$ human leukocytes, confirming repopulation (hCD45 positive cell fraction area of 42.6%). Immunohistochemistry, hemalaun counterstain. **Figure 14**. Boxplot presenting the area in the thymus of NSG and hu-NSG mice covered by mCD45$^+$ cells (mCD45 positive cell fraction area in %). There is no significant difference in the percentage of mCD45$^+$ cells between the two groups of mice ($p = 0.533$).

Figures 15-17. Femoral bone marrow. **Figure 15**. NSG mouse. **a**. The bone marrow is cell-rich; all hematopoietic cells are represented. Hematoxylin and eosin (HE). **b**. There are abundant mCD45$^+$ leukocytes. Immunohistochemistry, hemalaun counterstain. **Figure 16**. hu-NSG mouse. **a**. The bone marrow is highly cellular; all hematopoietic cell lineages are represented. HE. **b**. The number of mCD45$^+$ cells is low, positive cells are often apoptotic (arrowheads, also in inset). **c**. The majority of cells are hCD45-positive. Immunohistochemistry, hemalaun counterstain. **Figure 17**. Boxplot presenting the area in the bone marrow of NSG and hu-NSG mice covered by mCD45$^+$ cells (mCD45 cell fraction area in %). A significantly ($p = 0.006$) lower percentage of mCD45$^+$ cells is present in hu-NSG mice.

Figures 18-24. Granulomatous inflammation, hu-NSG mouse. **Figure 18**. Liver. There are multifocal inflammatory infiltrates, mainly arranged around portal areas. *, portal vein. Hematoxylin and eosin (HE). **Figure 19**. Liver. Cells in the focal infiltrates predominantly have the morphology of macrophages and lymphocytes (a, HE) and

almost all are Ku80-positive (b), confirming their human origin. These cells include numerous T cells (c, $CD3^+$) and fewer B cells (d, $CD20^+$). Immunohistochemistry, hemalaun counterstain. **Figure 20**. Bone marrow. **a**. Within the hematopoietic tissue are variably sized aggregates of larger mononuclear cells (arrows). HE. **b**. The majority of cells in such focal aggregates express MHC II, suggesting that there are abundant macrophages and activated lymphocytes. Immunohistochemistry, hemalaun counterstain. **Figures 21, 22**. Spleen. The red pulp is widely replaced by large granulomatous infiltrates (Fig. 21, arrows) including epithelioid cells (Fig. 22, arrowhead) and multinucleated cells (Fig. 22, arrow). HE. **Figures 23, 24**. Cervical lymph node. The normal architecture is widely replaced by granulomatous infiltrates (*). HE.

.

Figures 25-28. Comparison of efficiently humanized mice (hu-NSG(e), Figures 25 and 27) and inefficiently humanized mice (hu-NSG(i), Figures 26 and 28). **Figures 25, 26**. Proportion of human cells in the blood ($hCD45^+$, FACS) and lymphoid organs ($hCD45^+$, immunohistochemistry). Each symbol and line represents one individual. Note the large variability among the different individuals but also among different organs of a single individual. Grouping of the mice followed FACS analysis (cut off 15% hCD45). Lymph node values include the average of all detected lymph nodes in each animal (axillary, cervical and mesenteric). Animals with granulomatous inflammatory infiltrates are marked with an asterisk. Only organs without lesions were evaluated. **Figures 27, 28**. Proportion of human cells in the blood ($hCD45^+$, FACS) and bone marrow ($Ku80^+$, immunohistochemistry). Each symbol and line represents one individual. Note the large variability among the different individuals but also among different organs of a single individual, especially in the group of hu-NSG(i)

mice. Animals with granulomatous inflammatory processes are marked with an asterisk in Figures 25 and 26.

Supplemental figures

Figures S1, 2. T cell lymphoblastic lymphoma, thoracic cavity, NSG mouse, 6 months, female. **Figure S1**. Thoracic mass composed of a monomorphic neoplastic cell population that also infiltrates the adjacent mediastinal adipose tissue. HE stain. **Figure S2**. **a**. Neoplastic cells are arranged in tightly packed sheets and display scant amphophilic cytoplasm, round nuclei, and moderate anisocytosis. There are several mitotic (arrows) and apoptotic (arrowheads) cells. HE stain. **b**. The vast majority of neoplastic cells express the pan T cell marker CD3. **c**. Neoplastic cells are also CD4 positive (pink reaction along the cell border), but CD8 negative (no cells with blue reaction along the cell border). Immunohistochemistry, hemalaun counterstain.

Table 1. Antibodies and detection methods used for immunohistochemistry.

Antigen	Cells detected (human, murine)	Antibody (clone)	Antigen retrieval	Detection method
hCD45	Human leukocytes	pAB rabbit anti-human CD45[a]	CB pH 6.0, 96°C, 30 min	1:500, 60 min, RT, HRP Envision Rb[e]
mCD45	Murine leukocytes	mAB rat anti-mouse CD45 (I3/2.3) [a]	CB pH 6.0, 96°C, 30 min	1:100, ON, RT, HRP Envision Rb[e]
Ku80	Human cells	mAB rabbit anti-human Ku80 (C48E7)[b]	TE pH 9.0, 96°C, 30 min	1:200, ON, 4 °C, HRP Envision. Rb[e]
Iba1	Human and murine macrophages	pAB rabbit anti-human Iba1[c]	CB pH 6.0, 96°C, 30 min	1:750, 60 min, RT, HRP Envision Rb[e]
F4/80	Mature murine macrophages	mAB rabbit anti-mouse F4/80 (SP115)[d]	TE pH 9.0, 96°C, 30 min	1:150, 2 h, 37 °C, Omni Ultra Map Kit Rb (Discovery)
Lysozyme	Human and murine macrophages, neutrophils	pAB rabbit anti-human lysozyme[e]	Proteinase K[e], RT, 5 min	1:400, 60min, RT, HRP Envision Rb[e]
CD45R	Murine B cells, reported to cross react with human	mAB rat anti-mouse CD45R/B220 (RA3-6B2)[f]	CB pH 6.0, 96°C, 30 min	1:800, 60 min, RT, HRP Envision Rb[e]
CD3	Human and murine	mAB rabbit anti-mouse CD3 (SP7)[g]	TE pH 9.0, 96°C, 30 min	1:900, 1 h, 37 °C, Omni Ultra Map Kit Rb (Discovery)
Calprotectin	T cells Human and murine granulocytes, monocytes, macrophages	mAB mouse anti-human S100A8/A9 (MAC387)[a]	CB pH 6.0, 96°C, 30 min	1:100, 30 min, RT, Omni Ultra Map Kit Rb (Discovery)
CD4	Human and murine	mAB rabbit anti-mouse	CB pH 6.0	1:250, 1 h, RT,

	T helper cells	CD4 (EPR19514)[a]	RT, 2 h	HRP Envision Rb[e]
CD8	Human and murine cytotoxic T cells	mAB rabbit anti-mouse CD8 (D4W2Z)[b]	CB pH 6.0 100°C, 20 min	1:50, 10 min, RT, Refine Detection Kit Mixed DAB[h]
CD20	Human and murine B cells	pAB rabbit[a]	CB pH 6.0 100°C, 20 min	1:400, 37°C, 1 h, Omni Ultra Map Kit Rb (Discovery)
MHC II	Murine MHC II	mAB rat anti-mouse MHC II (NIMR-4)[a]	CB pH 6.0 98°C, 20 min	1:150, 60 min, RT, HRP Envision Rb[e]

Legend: mAB – monoclonal antibody; pAB – polyclonal antibody; CB – citrate buffer; TE – Tris-EDTA buffer; ON – overnight; RT – room temperature; Rb - rabbit

Commercial providers:

[a]Abcam, Cambridge, UK

[b]Cell Signaling Technology, Leiden, The Netherlands

[c]WAKO, Osaka, Japan

[d]Invitrogen/Thermo Fisher Scientific, Waltham, MA, USA

[e]Dako, Glastrup, Denmark

[f]BD Pharmigen, Franklin Lakes, USA

[g]Spring Bioscience, Ventana Medical Systems, Tucson, USA

[h]Leica Biosystems, Wetzlar, Germany

Table 2. Antibodies applied in the FACS analysis to detect human cells.

Antigen	Cells detected	Antibody and fluorophore (clone)	Dilution
CD45	Leukocytes	mAB hCD45 Pacific Blue (HI30)[a]	1:500
CD3*	T cells	mAB CD3 PE (UCHT1)[a]	1:100
		mAB CD3 BV785(OKT3)[a]	1:100
CD4*	T helper cells	mAB CD4 APC-Cy7 (RPA-T4)[a]	1:100
		mAB CD4 BV605 (OKT4)[a]	1:100
CD8*	Cytotoxic T cells	mAB CD8 PerCP (SK1)[a]	1:100
HLA-DR*	Activated leukocytes	mAB HLA-DR FITC (L243)[a]	1:200
		mAB HLA-DR PE-Dazzle 594 (L243)[a]	1:200
CD19*	B cells	mAB CD19 Pe-Cy7 (HIB19)[a]	1:100
		mAB CD19 A700 (HIB19)[a]	1:50
NKp46*	NK cells	mAB NKp46 APC (9E2)[b]	1:100

Legend: mAB – mouse monoclonal antibody

*Analysis was conducted after gating for hCD45 in order to only include human cells for subsequent FACS analysis.

Commercial Providers:

[a]Biolegend, San Diego, USA

[b]BD Pharmigen Franklin Lakes, USA

Table 3. Spectrum of histopathological lesions in male and female NSG and hu-NSG mice

NSG mice, aged 1-3 months (n=10) and 6 months (n=38) and hu-NSG mice, aged 3-6 months (n=61)

Organs (alphabetical order) and histological findings	NSG Males	NSG Females	Hu-NSG Males	Hu-NSG Females
Adrenal glands				
Subcapsular cell hyperplasia	5/28 (18%)	11/16 (69%)	10/22 (45%)	24/25 (96%)
Extramedullary hematopoiesis	2/28 (7%)	-	-	-
Angiectasis (corticomedullary junction)	-	2/16 (13%)	-	4/25 (16%)
Accessory cortical tissue	-	2/16 (13%)	1/22 (4.5%)	2/25 (8%)
Bones and joint				
Intersternebral joint degeneration	1/28 (4%)	-	-	-
Femoral articular cartilage degeneration (clefts)	3/30 (10%)	-	-	1/15 (7%)
Intervertebral joint degeneration	1/30 (3%)	-	-	-
Focal cortical thickening of femoral diaphysis	3/30 (10%)	1/15 (7%)	-	-
Bone marrow (sternum and femur)				
Hemosiderosis	6/31 (19%)	6/15 (40%)	-	-
Fatty infiltration (femur only)	5/30 (17%)	11/15 (73%)	4/14 (29%)	8/15 (53%)
Myeloid hyperplasia	1/31 (3%)	-	1/27 (4%)	1/28 (4%)

Granulomatous inflammation (human cells) [a]	-	-	8/27 (30%)	4/28 (14%)
Eyes				
Impaired retinal development	-	-	16/22 (73%)	18/24 (75%)
Cataract	-	-	3/22 (14%)	1/24 (4%)
Kidneys				
Tubular dilation with epithelial cell hypertrophy	4/31 (13%)	1/17 (6%)	2/31 (6%)	1/30 (3%)
Tubular basophilia	2/31 (6%)	1/17 (6%)	-	3/30 (10%)
Radiation nephropathy	-	-	4/31 (13%)	5/30 (17%)
Granulomatous inflammation (human cells) [a]	-	-	2/31 (6%)	2/30 (7%)
Liver				
Multifocal lymphohistiocytic cell aggregates (human cells) [a]	-	-	8/31 (26%)	5/30 (17%)
Granulomatous inflammation (human cells) [a]	-	-	5/3 (16%)	5/30 (17%)
Extramedullary hematopoiesis	-	-	7/31 (23%)	8/30 (27%)
Focal hepatocellular necrosis	-	-	1/31 (3%)	-
Lungs				
Alveolar macrophage aggregation with pleural thickening	24/31 (77%)	11/17 (65%)	29/31 (94%)	26/30 (87%)
Hair shaft granuloma	1/31 (3%)	-	-	-

Multifocal lymphohistiocytic cell aggregates (human cells) [a] with alveolar hemorrhage and fibrin deposition	-	-	9/31 (29%)	4/30 (13%)
Ovaries				
Atrophy		-		24/27 (89%)
Pancreas				
Acinar atrophy with chronic inflammation	1/31 (3%)	-	1/22 (5%)	-
Multifocal lymphohistiocytic cell aggregates (human cells) [a]	-	-	1/22 (5%)	2/24 (8%)
Salivary gland (mandibular)				
Acinar atrophy with chronic inflammation	-	-	1/22 (5%)	-
Chronic inflammation, due to foreign body (hair)	-	1/17 (6%)	-	-
Skeletal muscle				
Myofiber degeneration with inflammation, retroorbital muscle	-	1/17 (6%)	-	-
Myofiber degeneration with inflammation, masticatory muscle	1/31 (3%)	-	1/21 (5%)	-
Skin				
Interface dermatitis with scleroderma	-	-	4/19 (21%)	-
Neutrophilic inflammation, hair follicle, muzzle	-	1/17 (6%)	-	-
Spleen				
Extramedullary hematopoiesis	31/31 (100%)	15/15 (100%)	28/29 (97%)	29/29 (100%)

Hemosiderosis	10/31 (32%)	12/15 (80%)	1/29 (3%)	9/29 (31%)
Granulomatous inflammation (human cells)[a]	-	-	3/29 (10%)	3/29 (10%)
Testes				
Seminiferous tubule degeneration with mineralization	13/31 (42%)		10/22 (45%)	
Thymus				
Cysts	9/16 (56%)	8/13 (62%)	7/15 (47%)	7/15 (47%)
Thymus/mediastinal lymph node[b]				
Precursor T cell lymphoblastic lymphoma	-	1/13 (8%)	-	-
Uterus				
Glandular dilation with luminal debris		5/17 (29%)		-

[a]: Ku80-positive infiltrates; see also Table 5.

Numbers in parenthesis represent the number of animals exhibiting the specific lesion over the number of examined animals

[b]: Tissue of origin could not be determined

Table 4. Human cells in the lymphoid organs of efficiently and inefficiently humanized NSG mice. The area covered by human cells (hCD45+) in spleen, lymph nodes, thymus, and the number of Ku80-positive human cells in the bone marrow was measured. Significant differences between hu-NSG(e) and hu-NSG(i) were tested using t test.

Organ	**Hu-NSG(e) (n=8)**			**Hu-NSG(i) (n=8)**			
	Range (%)	**Mean (%)**	**SD ±**	**Range (%)**	**Mean (%)**	**SD±**	**P-value**
Spleen	8.4 - 46.8	21.0	13.9	0.1 - 35.5	8.8	12.8	p = 0.87
LN[a]	41.8 - 59.5	54.1	6.5	0.0 - 51.2	18.6	24.3	**p = 0.008**
Thymus	27.9 - 65.2	46.1	11.8	0.0 - 65.2	16.5	27.5	**p = 0.030**
BM[b]	42.3 - 88.4	69.6	15.0	0.5 - 56.3	28.2	23.3	**p = 0.001**

hu-NSG(e) and hu-NSG(i) mice: efficiently and inefficiently humanized NSG mice were defined as more than 15% and less than 15% hCD45$^+$ cells in the blood at the age of three months, respectively

LN - lymph nodes; BM - bone marrow

[a]The mean of hCD45+ area of the detected, i.e. histologically examined lymph nodes in each animal was taken for the calculation.

[b]hu-NSG mice: n = 12; hu-NSG(i) mice: n = 4

Significant values are highlighted in bold.

Table 5. Incidence and severity of granulomatous and/or mononuclear inflammatory infiltration (mediated by human cells) in the organs of hu-NSG mice.

Organ	Sex	Granulomatous inflammatory infiltration				
		Minimal	Mild	Moderate	Marked	Severe
Bone marrow	Male	2	1	3 (1)	-	1 (1)
	Female	2	-	-	1 (1)	1 (1)
Kidneys	Male	3	2 (2)	-	-	-
	Female	1	1 (1)	-	-	-
Liver	Male	1	-	3 (1)	1 (1)	
	Female	-	2	2 (1)	1 (1)	-
Lungs*	Male	-	3 (1)	1 (1)	-	-
	Female	1	1 (1)	-	-	-
Lymph nodes	Male	-	3 (2)	2	-	-
	Female	1	1 (1)	-	-	-
Skin*	Male	2 (1)	2	-	-	-
	Female	-	-	-	-	-
Spleen	Male	-	1	1 (1)	-	1 (1)
	Female	1 (1)	-	-	-	-

*Lesions were dominated by mononuclear cell infiltrates without typical granulomatous character.

Numbers give the total numbers of affected animals; numbers in brackets indicate how many of the affected animals had been euthanized due to clinical disease prior to the end of the experiment.

Table 6. Cellular composition of peripheral blood in animals with and without granulomatous inflammation (GI).

Cell type	Control group Mean (± SD)	Granulomatous inflammation Mean (± SD)	P-value and tendency (GI vs non-GI)	
Leukocytes[a]	63.1% (13.0)	39.0% (21.3)	0.002	↓
Lymphocytes[b]	74.9% (12.5)	53.0% (21.0)	0.003	↓
T cells (CD3+)	26.2% (10.6)	35.9% (20.1)	0.040	↑
B cells (CD19+)	66.5% (11.5)	26.1% (9.8)	0.020	↓
Activated T cells (CD3+/HLA-DR+)[c]	5.7% (5.0)	20.5% (12.3)	0.001	↑
Activated T helper cells (CD4+/HLA-DR+) [c]	3.4% (2.7)	14.4% (13.3)	0.010	↑
Activated cytotoxic T cells (CD8+/HLA-DR+) [c]	9.6% (9.3)	29.6% (19.5)	0.003	↑
Monocytes[d]	1.7% (0.6)	4.6% (2.8)	0.002	↑

Human leukocytes (a) were identified based on the expression of hCD45. The hCD45+ cells were subsequently separated further into lymphocytes (b) based on their size in the forward and sideward scatter, as well as T and B cells based on the expression of CD3 and CD19, respectively. HLA-DR co-expression identified activated T cells, activated T helper and activated T killer cells (c), whereas monocytes (d) were cells negative for all other markers, but HLA-DR positive. Statistical analysis was done using t test.

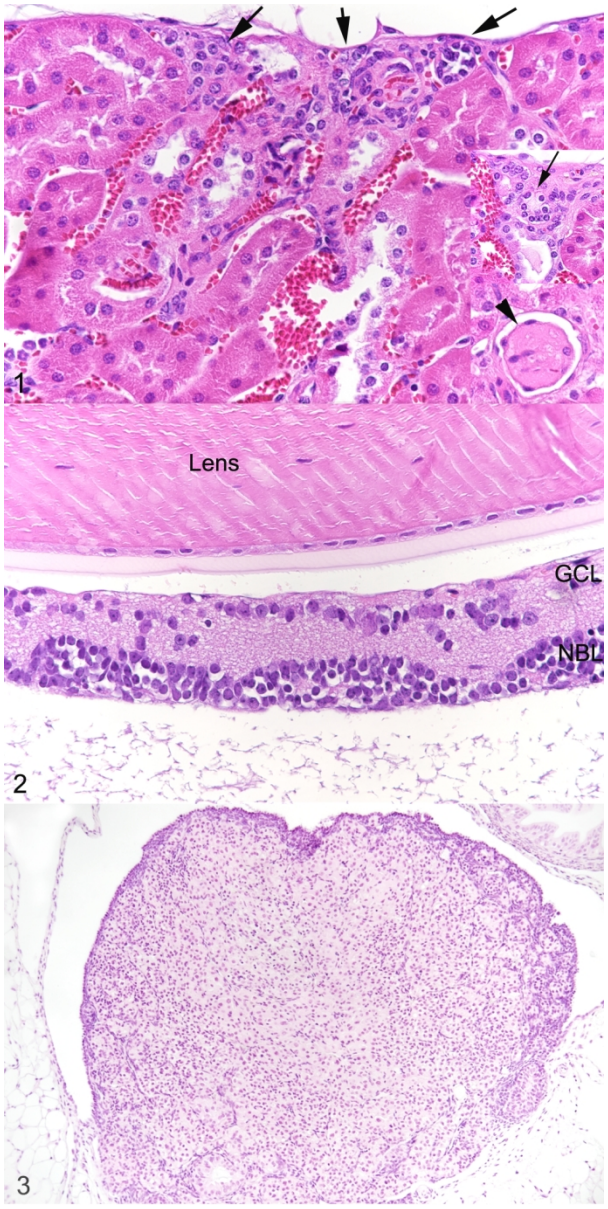

90x179mm (300 x 300 DPI)

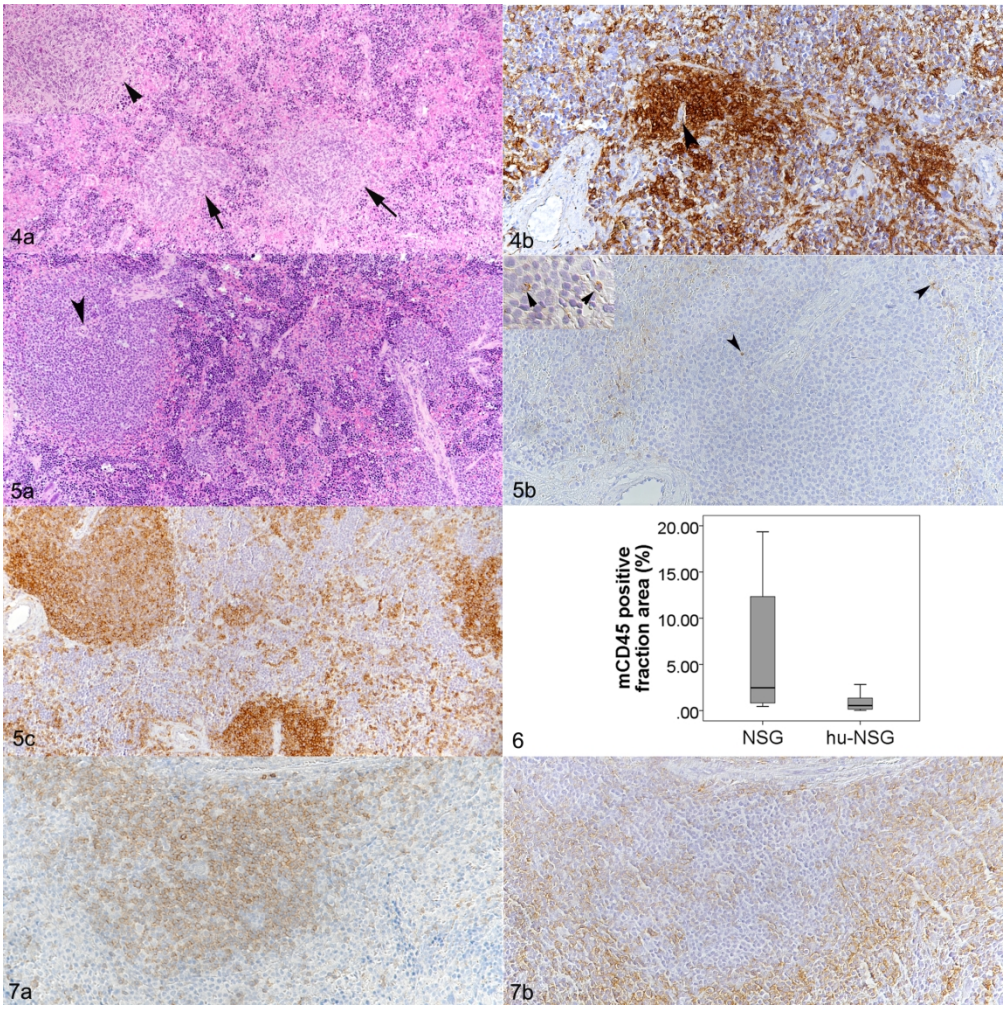

180x180mm (300 x 300 DPI)

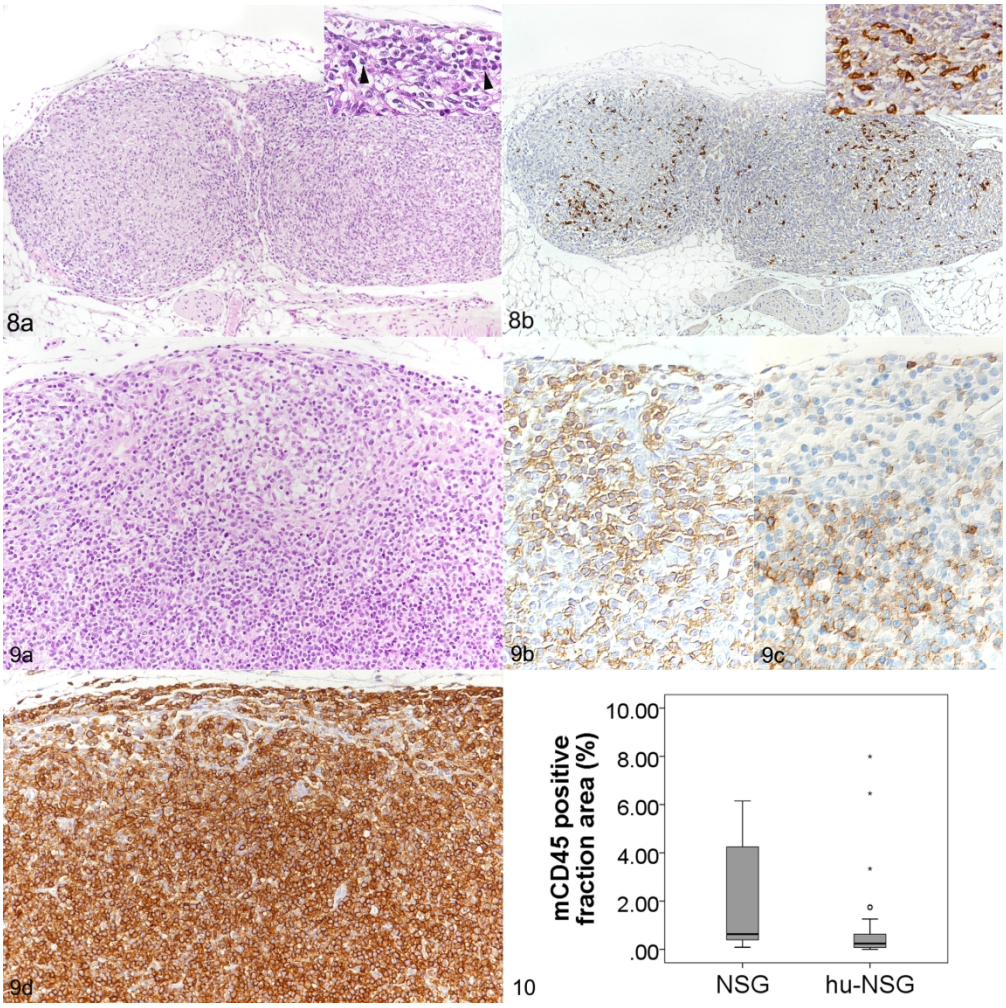

180x179mm (300 x 300 DPI)

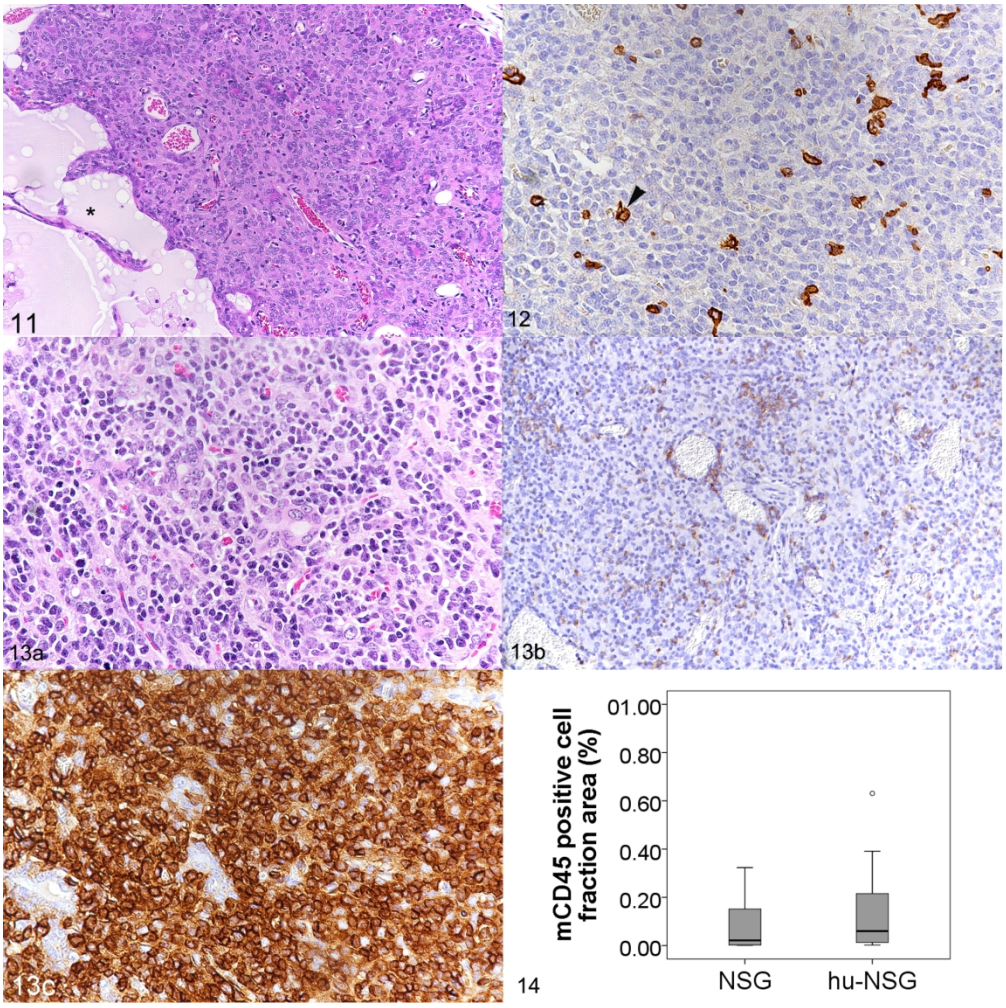

180x179mm (300 x 300 DPI)

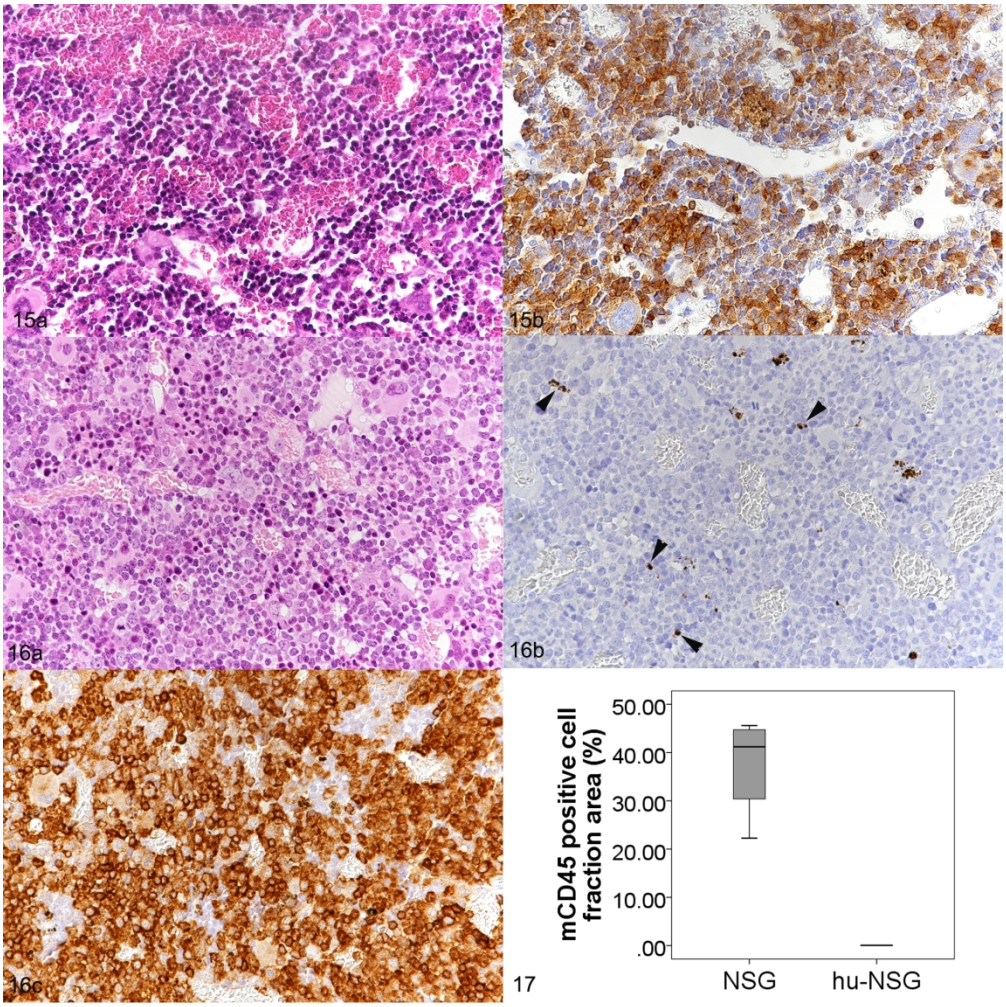

180x179mm (300 x 300 DPI)

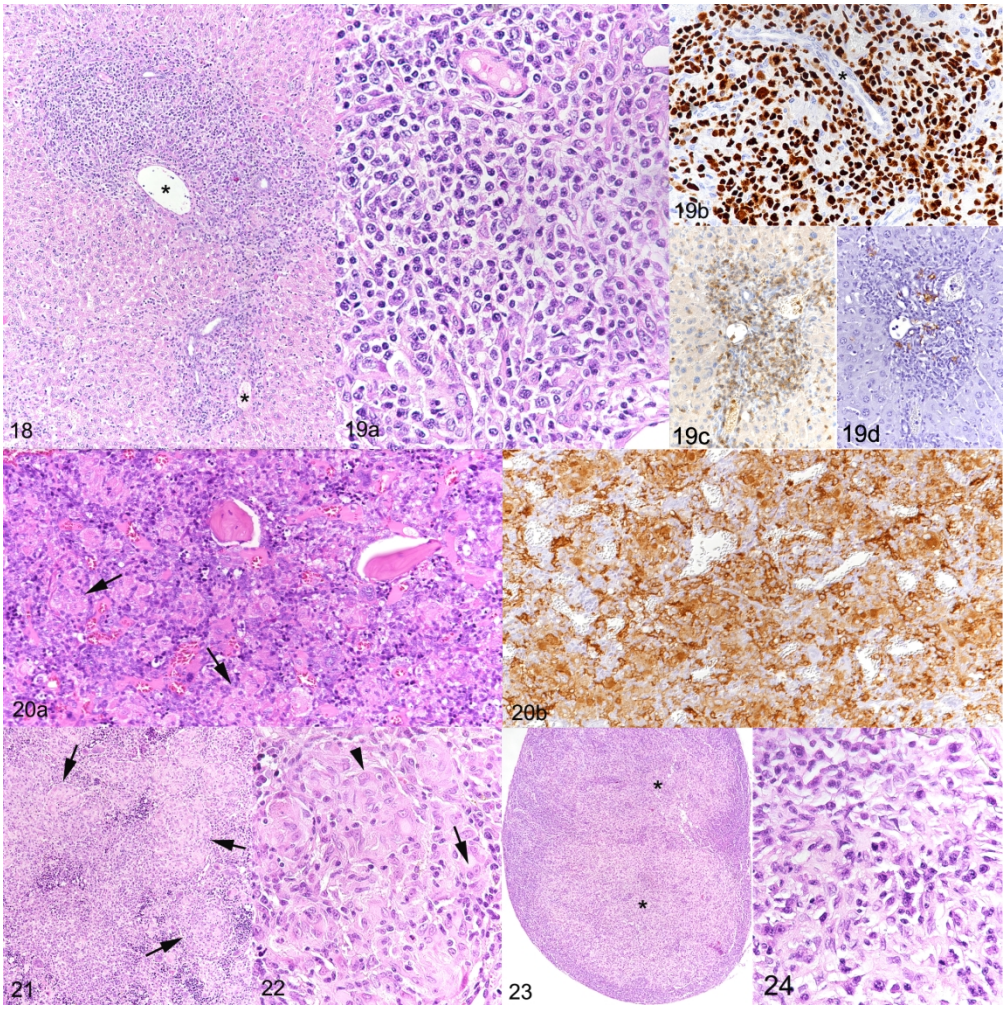

180x180mm (300 x 300 DPI)

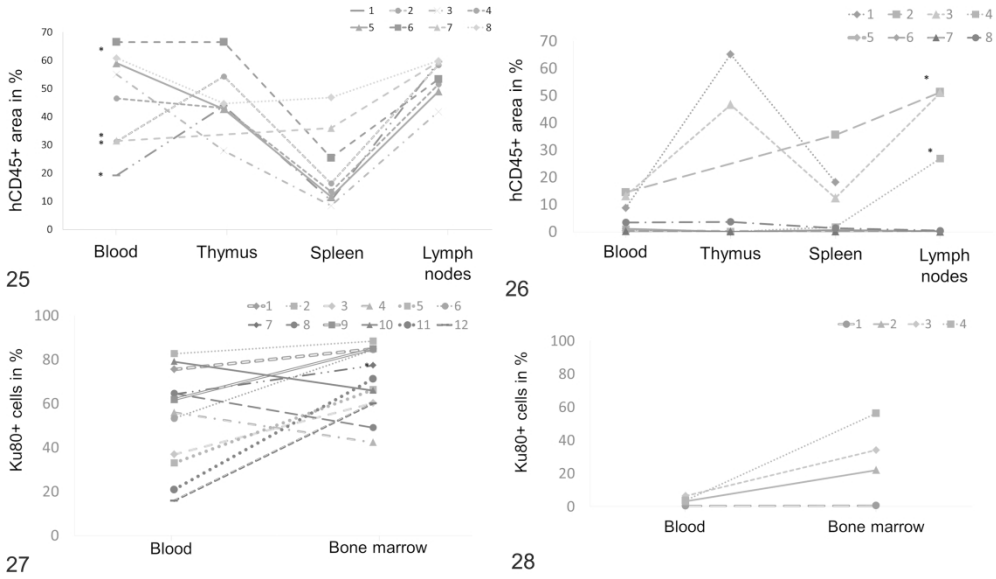

180x105mm (600 x 600 DPI)

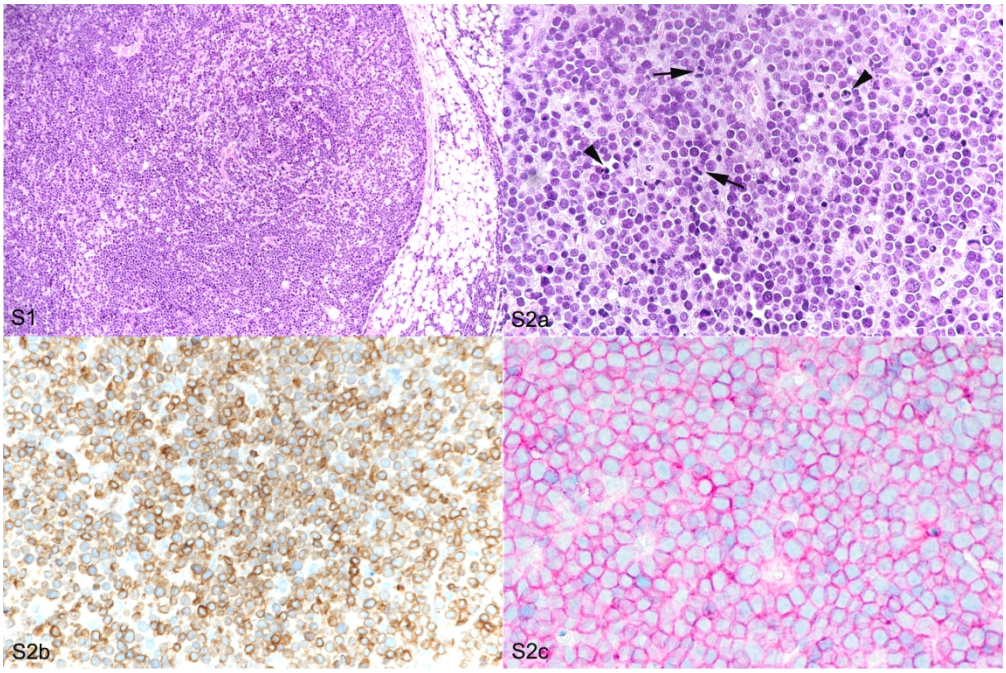

180x119mm (300 x 300 DPI)

Human CD34^{+} hematopoietic stem cell-engrafted NSG mice: Morphological and immunophenotypic features

Sandra Blümich, Hana Zdimerova, Christian Münz, Anja Kipar, Giovanni Pellegrini

Laboratory for Animal Model Pathology (LAMP), Institute of Veterinary Pathology, Vetsuisse Faculty, University of Zurich, Zurich, Switzerland (SB, AK, GP)

Viral Immunobiology, Institute of Experimental Immunology, University of Zurich, Zurich, Switzerland (HZ, CM)

Corresponding author:

Anja Kipar

Institute of Veterinary Pathology

Vetsuisse Faculty

University of Zurich

Winterthurerstrasse 268

CH - 8057 Zurich

Switzerland

Phone: 41 44 635 85 51

Fax: +41 44 6358934

E-mail address: anja.kipar@uzh.ch

Abstract

Immunodeficient mice engrafted with human immune cells represent an innovative tool to improve translatability of animal models for the study of human diseases. Immunophenotyping in these mice focuses on engraftment rates and cellular differentiation in blood and secondary lymphoid organs, and is predominantly carried out by FACS analysis; information on the morphological aspects of engraftment and the prevalence of histologic lesions is limited.

We histologically examined 3-6-month-old NSG mice, naïve or engrafted with $CD34^+$ human hemopoietic stem cells (HSC), and employed a quantitative immunohistochemical approach to identify human and murine cell compartments, comparing the results with the FACS data.

NSG mice mainly exhibited incidental findings in lungs, kidneys, testes and adrenal glands. A 6-month-old NSG mouse had a mediastinal lymphoblastic lymphoma. The lymphoid organs of NSG mice lacked typical lymphoid tissue architecture but frequently exhibited small periarteriolar leukocyte clusters in the spleen. Mice engrafted with human HSC frequently showed nephropathy, ovarian atrophy, cataract and abnormal retinal development, lesions considered secondary to irradiation. In addition, 20% exhibited multisystemic granulomatous inflammatory infiltrates, dominated by human macrophages and T cells, leading to the observed 7% mortality and morbidity. Immunophenotypic data revealed variable repopulation of lymphoid organs with $hCD45^+$ human cells, which did not always parallel the engraftment levels measured via FACS.

The study describes the most common pathological features in young NSG mice after human HSC engraftment. As some of these lesions contribute to morbidity, morphological assessment of the engraftment at tissue level might help improve immunophenotypic evaluations of this animal model.

Keywords: NSG mice, non-obese diabetic mice, Prkdc^{scid}, IL-2Rγ^{nul}, CD34^{+} stem cells, engraftment, humanized mice, granulomatous inflammation, graft versus host disease, lymphoma, radiation nephropathy.

Recent advances in the generation of humanized murine models, featuring immunodeficient mice engrafted with human immune system cells, have brought tangible breakthroughs in numerous research fields, such as the preclinical development of immunotherapeutic agents and the study of infectious, metabolic and autoimmune diseases. Progress has been facilitated by the optimisation of immunodeficient mouse models, which, being deprived of acquired and innate immunity, can be transplanted with human cells that eventually develop into a variably functional immune system in the model.[9,45,57,61]

Among the numerous immunodeficient mouse strains available, the NOD-scid IL-2Rγ^{null} (NSG) mouse is currently the most widely used for successful humanization of the immune system, showing one of the highest engraftment rates among the various strains.[29,64] NSG mice are non-obese diabetic (NOD) mice bearing the Prkdc^{scid} mutation and a genetic deletion of the common γ chain of the IL-2 receptor. Accordingly, they exhibit defects in lymphoid cell development, lacking both innate and adaptive lymphocytes, and have diminished complement activity due to C5 deficiency.[9,24,52] In contrast to their NOD/scid predecessors, NSG mice are not prone to develop thymic lymphoma; they have a long life span of about two years.[9,23]

Functional immune system abnormalities in immunodeficient mice are associated with abnormal development of the primary and secondary lymphoid organs; however, the morphological equivalents of the latter vary across the available models.[49] NSG mice, for example, exhibit a small spleen, thymus and lymph nodes that lack lymphoid structures and are composed almost exclusively of reticular stromal cells.[47,51,52]

Immunodeficient mice can be transiently or stably humanized by administration of human mature lymphoid or CD34^{+} hematopoietic stem cells (HSC), respectively.[61] Most models allow multi-lineage human immune cell engraftment and both the

acquired and innate human immune system components develop to variable degrees. The present study focuses on $CD34^+$ HSC humanized NSG (hu-NSG) mice, a model in which T and B cell engraftment is generally successful, though without consistent immunoglobulin (Ig) class switching and mostly IgM production by B cells.[19,45,56] Hu-NSG mice have human dendritic cells, NK cells and myeloid cells including neutrophils.[25,35,60] However, the latter two are generally seen at low numbers, and seem to be defective in their maturation and function.[19,23,45,57] It has been shown that the transplanted human leukocytes form variably sized aggregates in the lymphoid organs of these mice, which in general do not exhibit distinctive secondary lymphoid structures such as lymphoid follicles in spleen and lymph nodes.[23,57,60] In the thymus, repopulation appears to be more efficient in immunodeficient mice transplanted shortly after birth, whilst in mice engrafted at adult age the thymus is less prone to support human cell engraftment.[7,62] In the bone marrow the proportion of lymphoid and myeloid cells varies, as different published studies indicate.[60,62]

Effective engraftment in hu-NSG mice is generally determined by fluorescent activated cell sorting (FACS) analysis of the blood, usually at 12-16 weeks post-engraftment. The FACS data suggest that the extent of engraftment can vary substantially depending on the age of the mice, the source and manipulation of the HSC, and the administration route.[23,26] So far, most of the immunophenotyping data that are available for these mice are based on FACS analyses, carried out on circulating and organ-specific immune cells at different endpoints.[7,26,39,56] Accordingly, there is very limited information concerning the *in situ* aspects of engraftment, in particular in the hemolymphatic tissues and, specifically, how these correlate with the engraftment rates and cellular differentiation determined by FACS. Furthermore, little is known about the incidence of spontaneous diseases and

common histopathological lesions in hu-NSG mice, and even in NSG mice. Information about the spectrum of histopathological lesions occurring spontaneously in NSG mice is mainly limited to the prevalence of neoplastic findings in the NOD background strain[22] or a few reports on the most common causes of mortality and morbidity and age-related lesions in old NSG mice housed in conventional mouse facilities.[16,47] In the few reports available about hu-NSG mice, spontaneous changes were generally mentioned alongside the findings relevant to the study instead of being a focus of investigation.[8,32,47,62] However, a recent study reported histological lesions that provide evidence of the occurrence of graft versus host disease (GvHD) in HSC hu-NSG mice.[11] Considering the increasing use of humanized mice in efficacy and safety studies, including regulatory safety assessment, this knowledge gap needs to be addressed and better characterization of the model is warranted to consolidate its translatability.

The present study aimed to characterize the morphological phenotype of NSG mice and their humanized counterpart, the CD34$^+$ hu-NSG murine model generated via perinatal intrahepatic injection of human CD34$^+$ fetal liver cells into NSG mice after preconditioning irradiation. We found high variability in the levels of human cell engraftment in the blood of hu-NSG mice within the same experiment and hypothesized that this is reflected by a similarly variable reconstitution in the lymphoid organs. Another purpose of this study was to assess the spectrum of histopathological lesions and identify the main causes of morbidity and mortality in young NSG and CD34$^+$ HSC hu-NSG mice, since, despite the increased popularity of these animal models in nonclinical testing, the published data on this topic is very sparse.

.

Materials and Methods

Animals

The study was undertaken on NOD-scid IL-2Rγ^{null} (NSG) mice from a breeding colony established in a research facility at the Institute of Experimental Immunology, University of Zurich, Switzerland from animals originally purchased from Jackson Laboratories (Bar Harbor, USA). Animals were housed in groups of up to five males or females respectively and fed *ad libitum* with conventional diet (M/R Haltung Extrudat, Alleinfuttermittel für Mäuse und Ratten, 3436; Granovit AG, Kaiseraugst, Switzerland). Water was provided *ad libitum*, the day and night cycle included 12 hours of light, from 6 am to 6 pm. The colony was maintained under specific pathogen-free conditions and sentinel animals were confirmed to be free of viral, bacterial, and parasitic pathogens listed in the FELASA recommendations,[37] except for mouse norovirus (MNV) and *Helicobacter*.

The study cohort comprised a total of 109 mice. Among these were 48 NSG mice (31 males, 17 females) that did not receive any treatment. Of these, 10 (6 males, 4 females) were culled at 1-3 months of age, representing animals bred for, but not used in humanization experiments. Thirty-eight (25 males, 13 females) were breeding animals that were culled at 6 months of age, at the end of their breeding career. The second cohort of 61 hu-NSG mice (31 males, 30 females) were subjected to human cell engraftment (inefficiently humanized mice at 3 months of age (n = 22; <15% hCD45^{+} cells in peripheral blood after reconstitution), and efficiently humanized mice at 4-5 months of age (n = 39)). These animals had served as the non-infected control group in an experiment to investigate the effects of Epstein-Barr virus infection on the immune system and were culled at the age of 3-5 months, at termination of the experiment. As part of the above-mentioned experiment on Epstein-Barr virus infection, the animals were injected intraperitoneally with 100 µl PBS at 12 to 14

weeks after irradiation. At the age of 4 months, 4 of these animals, 2 males and 2 females, developed progressive weight loss and signs of unease such as hunched posture, rough coat and reddened skin, and had to be euthanized.

After reconstitution, mice were clinically checked daily for three days, and then three times a week until weaning. A weekly check was performed on mice four weeks and older, including naïve NSG mice.

Human Tissue Engraftment

$CD34^+$ HSC were isolated from fetal livers (Advanced Bioscience Resources, CA, USA) following established protocols.[54] Cells originated from 13 different donors and were frozen in liquid nitrogen prior to their use in the engraftment experiments. At the age of 1-6 days, NSG mice (n=61) were each irradiated with 1Gy (preconditioning), using a “Rad Source 2000” equipped with an X-ray source, and injected intrahepatically 5-7 hours later with $1\text{-}3x10^5$ $CD34^+$ human HSC. After 10-12 weeks, blood was collected via the tail vein and analyzed by FACS. In addition to the above reported morbidity after 4 months, 6% of irradiated and reconstituted hu-NSG pups were lost prior to weaning due to neglect or cannibalism by the mother. It remains unclear if this was connected to irradiation and/or reconstitution.

Ethics Statement

All animal protocols were in accordance with the Swiss Animal Welfare Act, Tierschutzgesetz (TSchG) and were approved by the veterinary office of the canton of Zurich, Switzerland (protocols 148/2011, 209/2014 and 159/17). The studies involving human samples were reviewed and approved by the cantonal ethics committee of Zurich, Switzerland (protocol KEK-StV-Nr.19/08, KEK-ZH-Nr. 2010-0057 and 2019-00837).

Macroscopic and Histological Examination

Mice were euthanized by 100% carbon dioxide asphyxiation, followed by exsanguination and creation of a pneumothorax. A full necropsy was conducted on each mouse and a standard selection of organs, hemolymphatic tissues, as well as bones and joints were sampled and fixed in 10% neutral buffered formalin for 48-120 hours, then trimmed and routinely embedded in paraffin wax following a predefined blocking pattern. Consecutive sections (3-5 µm) were prepared and routinely stained with hematoxylin and eosin (HE), special stains (when appropriate) or subjected to immunohistochemistry. Examined tissues were adrenal glands, brain, eyes, female genital tract (mammary gland, ovaries, uterus, vagina), gastrointestinal tract (stomach, duodenum, jejunum, ileum, cecum, colon and rectum), Harderian gland, heart, kidneys, liver with gall bladder, lungs, male genital tract (epididymis, prostate, testes, seminal vesicles), pancreas, salivary glands, skeletal muscle (*Musculus quadriceps femoris*), skin, spinal cord, tongue, and urinary bladder. Examined hemolymphatic tissues were bone marrow from several locations (see bones), lymph nodes [cervical (one lymph node of the cervical chain: mandibular, accessory mandibular or superficial parotid), mesenteric (colic or jejunal), proper axillary] (in most animals, not all three lymph nodes were successfully sampled as these could not be identified grossly), spleen (1-2 cross sections), and thymus. Since thymus and lymph nodes were difficult to grossly identify especially in NSG mice, tissue in the corresponding area was collected and included in the paraffin block. Bones (sternum, femur and tibia with femorotibial joint, spinal column) as well as the head with nasal and oral cavities and teeth were also collected. After fixation, these were decalcified for 3-5 days in a mild decalcifying solution (RDF, Mild Decalcifier, CellPath, Newtown, UK), followed by paraffin embedding. Special stains were applied when considered

necessary and comprised the Gram, Giemsa, Grocott, and Ziehl-Neelsen stains as well as the periodic acid-Schiff reaction).

Immunohistochemistry

Immunohistochemistry was applied to detect cells of human origin (Ku80$^+$), human and mouse leukocytes (hCD45$^+$, mCD45$^+$), T cells (CD3$^+$, CD4$^+$, CD8$^+$), human and mouse B cells (CD20$^+$ andCD45R-B220$^+$, respectively, monocytes/macrophages (calprotectin$^+$, Iba1$^+$, F4/80$^+$, lysozyme$^+$) and MHC II expression. Antibodies and detection methods are listed in Tables 1 and 2.

Histological Scoring and Histomorphometry

All tissues/organs were examined for histopathological changes which were diagnosed following the International Harmonization of Nomenclature and Diagnostic Criteria (INHAND), Society of Toxicological Pathology (www.toxpath.org/inhand.asp). When appropriate, lesions were graded semi-quantitatively using a score from 1 to 5. Granulomatous inflammation scores were primarily determined by the amount of tissue involvement (1 = minimal [< 1%]; 2 = mild [1–25%]; 3 = moderate [26–50%]; 4 = marked [51–75%]; 5 = severe [76–100%]) as described.[50]

For morphometric evaluation, slides with hemolymphatic tissue sections stained by immunohistochemistry were scanned using a digital slide scanner (NanoZoomer-XR C12000, Hamamatsu Photonics K.K., Iwata City, Japan), the Visiopharm Integrator System (Visiopharm, Hoersholm, Denmark) was used for the subsequent quantitative analysis. The mCD45 and hCD45 positive cell fraction areas and the number of Ku80 (nuclear marker) positive nuclei per high power field were calculated on consecutive sections. The mCD45 positive cell fraction area in hemolymphatic organs

repopulated by human cells was calculated following subtraction of the hCD45 positive area from the total tissue area.

FACS Analysis

FACS served to identify hCD45$^+$, CD3$^+$, CD4$^+$, CD8$^+$, CD19$^+$, NKp46$^+$, CD4/DR$^+$, CD8/DR$^+$ populations and followed previously described protocols.[2] Peripheral blood was collected from hu-NSG mice 3 months after human cell engraftment by tail vein bleeding into heparin-containing tubes (Heparin-Na, Braun). After two rounds of red blood cell lysis, peripheral blood mononuclear cells (PBMCs) were washed with PBS and stained with fluorescence coupled antibodies for 20 minutes at 4 °C. Antibodies are listed in Table 2. Subsequently, cells were fixed in 4% paraformaldehyde diluted in phosphate buffered saline (PBS) for 0 to 24 hours. Data was acquired on the BD FACSCanto II using DIVA software and analysed using FlowJo software Version 10.2. The cells were first gated for singlets, followed by hCD45.

Statistical Analysis

Statistical analysis was conducted using a Statistics Software (SPSS, 23). Correlation between FACS results and abundance of hCD45 positive cells in the lymphoid organ tissue sections was tested using Pearson test. Spearman's correlation analysis was used to study the relationship between granulomatous inflammation and activated T cells. For this analysis, granulomatous inflammation was divided in three categories as 0 = not present; 1 = mild, occurring with low severity and limited distribution; and 2 = severe , occurring with high severity and broad distribution. Statistical significance was evaluated using Mann-Whitney-U-Test and t-test. p values <0.05 were considered statistically significant.

Results

Background lesions and radiation-induced changes

The NSG mouse cohort (n = 48) remained healthy during the examination period and exhibited only a limited selection of histological lesions, with generally low severity (Table 3). The most frequently encountered changes were minimal or mild multifocal alveolar macrophage accumulation with pleural thickening in the lungs; minimal focal tubular basophilia and tubular dilation with epithelial cell hypertrophy in the kidneys; minimal or mild patchy degeneration and dystrophic mineralization of seminiferous tubules in the testes; and minimal to moderate multifocal subcapsular cell hyperplasia in the adrenal glands.[50] The latter occurred with higher frequency in females. Sporadically, minimal or mild focal degenerative changes in the intersternebral and intervertebral joints as well as cortical thickening of the femoral diaphysis were noted. Individual animals exhibited inflammatory processes, such as minimal focal neutrophilic myositis in retro-orbital and masticatory muscles, focal neutrophilic folliculitis in the skin of the muzzle, and a moderate diffuse chronic sialoadenitis. The latter appeared to be the consequence of an obstruction of the main excretory duct by a hair. Also, one mouse showed marked chronic pancreatitis, characterized by diffuse fibrosis, moderate mononuclear cell inflammation and lobular acinar atrophy. Apart from occasional dilation of endometrial glands, the female reproductive tract was free of histopathological changes. Ovaries exhibited numerous follicles at different stages of maturation and corpora lutea. The vagina showed normal cyclic changes consistent with all four phases of the rodent reproductive cycle.

The hu-NSG mice exhibited the same type of background lesions as the NSG mice, and with similar frequency and severity (Table 3). In addition, hu-NSG mice showed

histological changes consistent with exposure to radiation in the early postnatal period, i.e. radiation nephropathy, cataract and impaired retinal development,[4] and ovarian atrophy.[1,6] Radiation nephropathy was characterized as deposition of proteinaceous material and reduced number of capillaries in glomeruli, cortical tubular collapse[40], and was observed in relatively few mice (13% of males, 17% of females) and with minimal severity (Fig. 1). Impaired retinal development was more frequent (more than 70% of animals), and ranged from a thinning of the outer nuclear layer and the outer segment layer, to a lack of distinction between outer and inner nuclear layer, leading to a very thin retina composed of a single row of nuclei (Fig. 2). Changes were more severe in the peripheral portion of the retina. Cataract occurred in fewer mice (Table 3) with low severity and consisted of rupture of the posterior lens capsule with lens fibre fragmentation and focal liquefaction. Almost all female animals exhibited ovarian atrophy of varying degree. In more severe cases, the ovaries were reduced in size and exhibited a marked reduction to complete absence of oocytes, follicles and corpora lutea (Fig. 3). Such animals appeared to be in persistent anestrus, as there was no evidence of estrus cycling in uterus and vagina.

Hemolymphatic tissues

Spleens, lymph node, thymus and bone marrow were compared in both groups of mice, in particular to comparatively assess the murine and human leukocyte component in hu-NSG mice. Based on previous experience of the group, hu-NSG mice were classified as inefficiently humanized (hu-NSG(i) mice), when they exhibited less than 15% hCD45$^+$ cells in the blood (determined by FACS). This applied to 22/61 (40%) of the animals in the present study.

Spleen. In the NSG mice, spleens were generally small, less than 12 x 2 x 1 mm in size, with rare, randomly distributed leukocytes (mCD45$^+$) and no morphological

316 evidence of lymphocytes populating follicles and T cell zones. In 27/48 of the NSG
317 mice, small aggregates of mCD45$^+$ cells were found around one or two arterioles,
318 reminiscent of periarteriolar lymphoid sheaths (PALS; Fig. 4a, b). The aggregates
319 were composed of round to polygonal cells of approximately 15 µm diameter, with
320 scant cytoplasm and a large round to slightly elongated nucleus with finely stippled
321 chromatin and no evident nucleolus. These cells were consistently negative for T cell
322 (CD3), B cell (CD45R-B220) and macrophage (F4/80, calprotectin and lysozyme)
323 markers. The red pulp was mainly populated by erythroid progenitors and some
324 megakaryocytes, representing minimal to moderate extramedullary hematopoiesis
325 (Fig. 4a), and scattered leukocytes; some animals also exhibited minimal
326 hemosiderosis.
327 In all hu-NSG mice, the spleens were substantially larger, approximately 15 x 5 x 2
328 mm on average. Histologically, this was due to the much higher cellularity of the
329 organ secondary to human cell repopulation. While there was no evidence of
330 follicular structures, human cells tended to cluster around splenic arterioles, forming
331 PALS-like structures (Fig. 5) similar to but generally much larger than those formed
332 occasionally by mCD45$^+$ cells in the spleen of NSG mice. In the latter, due to the
333 PALS-like aggregates, the proportion of the area in the spleen covered by mCD45$^+$
334 cells averaged 6% (n = 6; mean = 6.3; SD = ±7.8), but exceeded 10% in individual
335 animals (Fig. 6), whereas murine leukocytes (mCD45$^+$) were extremely rare in hu-
336 NSG mice (Figs. 5b, 6). In contrast, they carried numerous hCD45$^+$ cells (Fig. 5c). In
337 efficiently humanized (hu-NSG(e)) mice, the hCD45-positive cell fraction area was
338 21.0% on average, though the proportion varied considerably between animals
339 (Table 4). In hu-NSG(i)mice, the hCD45 positive cell fraction area had a mean of
340 8.8% (Table 4); however, the difference between the two groups was not significant.
341 The white pulp in hu-NSG mice consisted of B cells (CD20$^+$) and T cells (CD3$^+$) in

342 equal proportions. The T cells were mostly found in the center of the reconstituted
343 white pulp, in the PALS-like structures around the arteries (Fig. 7a). B cells tended to
344 occupy the periphery of the white pulp but did not arrange in clear follicular structures
345 (Fig. 7b). Immunolabeling for CD4 and CD8 identified mainly $CD4^+$ T cells whereas
346 only random individual cells scattered throughout the parenchyma were $CD8^+$. In all
347 animals, the remaining area (red pulp) was mainly occupied by erythroid progenitor
348 cells, intermingled with megakaryocytes (moderate extramedullary hematopoiesis)
349 and scattered $hCD45^+$ leukocytes with the morphology of lymphocytes; these
350 appeared to be represented by B cells and T cells in equal proportions (Fig. 7).
351 **Lymph nodes**. In NSG mice, lymph nodes were generally very small and difficult to
352 identify grossly. However, in the majority of animals, the mesenteric and mandibular
353 lymph nodes were successfully sampled. They were composed predominantly of
354 connective tissue, i.e. the reticular stroma (Fig. 8a). Leukocytes ($mCD45^+$) were
355 present in low numbers, scattered throughout the fibrous scaffold (Fig. 8b). When
356 sampled successfully, axillary and inguinal lymph nodes exhibited the same
357 morphological features.
358 In hu-NSG mice, lymph nodes were in general larger and therefore easier to identify
359 grossly. Histologically, most lymph nodes were abundantly populated by lymphoid
360 round cells (Fig. 9). They contained only few murine leukocytes ($mCD45^+$; n = 33,
361 mean ± SD = 0.86 ± 1.8 %), and on average less than the lymph nodes of NSG mice
362 (n = 11; 2.8 ± 4.1%) (Fig. 10). Instead, human leukocytes ($hCD45^+$) repopulated the
363 fibrous stroma (n = 33; 42.1 ± 22.4%) (Fig. 9d). In efficiently humanized mice, the
364 hCD45-positive cell fraction area had a mean of 54.1%, whereas in inefficiently
365 humanized mice, the mean was 18.6% (Table 4). In some of the latter animals, no
366 human cells were identified at all; these lymph nodes had morphological features
367 identical to those of the NSG mice. However, also in the efficiently humanized mice,

repopulating hCD45$^+$ cells appeared to distribute randomly across the lymph node, did not aggregate to form appreciable lymphoid follicles or paracortical structures, and did not allow distinction of the cortex and medulla. Accordingly, CD20$^+$ B cells which were present in moderate to high numbers, and CD3$^+$ T cells which were slightly less numerous, were seen randomly distributed throughout the stroma. Overall, the periphery had a higher proportion of B cells (Fig. 9b) while T cells tended to be more numerous in the center (Fig. 9c). Most T cells appeared to be CD4$^+$, whereas CD8$^+$ cells were only present in very small numbers.

Thymus. In NSG mice, the thymus was generally barely visible and composed of hypoplastic lobules that lacked a defined cortex and medulla and often contained cysts, as previously reported (Fig. 11).[7] Again, leukocytes (mCD45$^+$) were rare (Fig. 12).

In hu-NSG mice, the thymus generally appeared slightly larger, with an approximate size of 2 x 1 x 1 mm. Lobules were more cellular and exhibited moderate numbers of lymphoid cells (Fig. 13), but still lacked the typical corticomedullary distinction. Murine leukocytes were rare (Fig.13b): the mCD45 positive cell fraction area had a mean of 0.4% (Fig. 14). Still, mCD45$^+$ cells were sometimes more numerous than in NSG mice, where the area covered by mCD45$^+$ cells did not exceed 0.3% (n = 9; mean ± SD = 0.09 ± 0.1 %) (Fig. 14). Repopulation with hCD45$^+$ leukocytes was variable in hu-NSG mice. In efficiently humanized mice (Fig. 13c), the mean of the hCD45 positive cell fraction area reached 46.1%, whereas it was 16.5% in inefficiently humanized mice (Table 3). The majority of these cells were CD3$^+$. Of this subpopulation, most cells were CD4$^+$ whereas CD8$^+$ cells were only visible in very small numbers. CD20$^+$ cells were barely present.

One 6-month-old female breeding NSG mouse exhibited a white-tan, firm mass of approximately 0.4 cm in diameter in the thoracic cavity. Histologically, it was

composed of dense sheets of large round neoplastic cells which also infiltrated the adjacent adipose tissue (Supplemental Fig. S1). The cells exhibited scant amphophilic cytoplasm and round nuclei with coarsely arranged chromatin. There was moderate anisocytosis and a mitotic rate of 2-4/HPF; a moderate number of apoptotic cells was observed (Supplemental Fig. S2a). The vast majority of cells were found to express CD3 and CD4 (Supplemental Fig. S2b, c), whereas B cells ($CD45R^+$) were seen in low numbers and randomly distributed. This led to the diagnosis of a precursor T cell lymphoblastic lymphoma.[38] It was not possible to determine whether the neoplasia originated from the thymus or the mediastinal lymph nodes. The mouse did not exhibit any additional histopathological changes.

Bone marrow. In NSG mice, the bone marrow (sternal and femoral) generally exhibited a high cellularity, represented by erythroid, $mCD45^+$ myeloid and megakaryocytic hematopoietic precursors (Fig. 15). Mild to moderate hemosiderosis as well as fatty infiltration (femur only) was occasionally seen (Table 2A).

In hu-NSG mice, the morphology of the bone marrow was similar, with high to very high cellularity (Fig. 16). While $mCD45^+$ cells were very rare, making up a significantly lower proportion of area than in the NSG mice (Fig. 16b, 17), $hCD45^+$ cells were the dominant cell population (Figs. 16c). The number of human cells ($Ku80^+$) was significantly higher in efficiently humanized vs inefficiently humanized mice (Table 4).

Granulomatous inflammation in $CD34^+$ hu-NSG mice

Two male and two female hu-NSG mice developed poor health before study completion and were electively euthanized, the females at 28 weeks after HSC transplantation due to severe progressive weight loss, and the males at 30 weeks. Both males were thin and exhibited clinical signs, i.e. hunched posture, rough coat

and reddened skin. All four mice exhibited grossly enlarged lymph nodes and spleen, diffusely pale bone marrow, and a red and white mottled liver. Histological examination revealed extensive granulomatous inflammatory infiltrates in these tissues as well as in the kidneys (Figs. 18-24). There was no evidence of bacterial or fungal organisms within the inflammatory infiltrates, as confirmed by various special stains (Gram, Giemsa, periodic acid-Schiff, Grocott, and Ziehl-Neelsen). [11,53]Granulomatous infiltrates were represented by multifocal to coalescing, partly nodular aggregates of macrophages and epithelioid cells, admixed with numerous lymphocytes and multinucleated giant cells (Figs. 18-24). In the infiltrates, cells were often found to proliferate, which was reflected by the presence of 1-3 mitotic figures per high power field. The vast majority of cells were human leukocytes ($Ku80^+$ (Fig. 19b), $hCD45^+$), with only very few intermingled murine ($mCD45^+$) leukocytes. Macrophages and T cells ($CD3^+$) dominated in the infiltrates which also contained a variable portion of B cells and a few viable neutrophils (Fig. 19c, d). Combined immunohistochemistry for CD4 and CD8 antigens revealed a striking predominance of $CD4^+$ T cells, with only rare CD8 or double-positive cells. In the liver, lesions consisted of lymphohistiocytic or granulomatous infiltrates that were mainly located in periportal areas (Figs. 18, 19a) and were associated with minimal to moderate deposition of fibrous connective tissue as well as scattered hemosiderin-laden macrophages. Bile ducts were often embedded within the inflammatory reaction, but were neither altered nor infiltrated, suggesting that they were not targeted by the inflammatory cells at this stage. Bone marrow changes presented as scattered nodules randomly distributed in the hematopoietic tissue (Fig. 20a) to subtotal replacement of the hematopoietic cell component by, in the majority, MHC II positive cells (Fig. 20b), with concurrent bone marrow necrosis and hemorrhage as well as trabecular bone resorption (data not shown). Affected spleens and lymph nodes

(Figs. 21-24) showed scattered focal infiltrates or severe disruption of the architecture by the inflammatory infiltrates. When affected, kidneys exhibited only mild changes, represented by scattered granulomatous foci randomly distributed throughout the cortical interstitium. In individual cases, pancreas, ovaries, serosae, Harderian glands, nose and/or oral cavity also showed granulomatous infiltrates.

Some animals with the above-described lesions also exhibited inflammatory infiltrates in lungs and skin. In the lungs, these represented peribronchiolar and perivascular aggregates of Ku80-positive cells, which were predominantly T cells and B cells, with fewer macrophages, occasionally containing golden brown pigment, and no evident giant cells. Infiltrates occasionally extended into the bronchiolar and alveolar lumina. In the skin, minimal or mild infiltration of Ku80-positive, predominantly $CD4^+$ and fewer $CD8^+$ T cells and rare B cells was seen at the dermo-epidermal junction, predominantly along the follicular dermo-epidermal junction, associated with vacuolar change and occasional apoptosis in the basal follicular keratinocytes and, to a lesser extent, the basal epidermal keratinocytes.

Granulomatous inflammatory infiltrates were also observed in mice without clinical signs, with lower severity and higher incidence in males (21%; 6/29) than in females (11%; 3/28). Liver, spleen, lymph nodes, bone marrow at different locations (sternum, femur and tibia, vertebrae and frontal bones in the skull) and kidneys were most consistently affected (Table 5). Prevalence and severity of the inflammatory infiltrates was comparable across all engrafted mice, with no obvious differences between the reconstitutions from different donors; however, this could not be specifically addressed due to the low number of mice reconstituted with the same donor.

Comparison of blood and lymphoid tissues

The FACS analysis performed on the peripheral blood of the hu-NSG mice revealed a large variability in the proportion of human leukocytes (hCD45$^+$), ranging from 0.14% to 66.5% (Figs. 25, 26). As mentioned above, mice with more than 15% hCD45$^+$ cells in the blood were considered as efficiently humanized (Figs. 25, 27), and below this threshold as inefficiently humanized (Figs. 26, 28).

Immunohistochemistry against hCD45 was performed on the lymphoid organs of a random selection of efficiently and inefficiently humanized mice (each n = 8) to correlate with the FACS data. As expected, this grouping of mice matched to some extent with the degree of repopulation of the hemolymphatic organs, as overall the percentage of human cells was significantly higher in lymph nodes, thymus and bone marrow of the efficiently compared to the inefficently humanized mice (Table 4). Interestingly, there was no substantial difference in the spleen. This may be due to the overall low relative extent of repopulation of this organ, which still contained a significant proportion of murine hematopoietic cells; even in efficiently humanized mice, the mean percentage area covered by human leukocytes (hCD45$^+$) was 21.0%, whereas it was 46.1% and 54.1% in thymus and lymph nodes respectively (Table 3). However, looking at repopulation levels in the different organs of individual animals it became obvious that there was substantial variation. The bone marrow was specifically analyzed because it can be expected to be most relevant for the production of cells that later appear in the blood stream. However, a mouse classified as inefficiently humanized could have a proportion of human cells in the bone marrow that was as high as that seen in efficiently humanized mice (Figs. 26, 28).

The FACS results of animals with evidence of granulomatous inflammation (n = 13) were compared with those of mice without such lesions (n = 48). Interestingly, animals with granulomatous inflammation were found to have significantly lower proportions of human leukocytes (Table 6). In the latter, the human leukocyte

population contained significantly lower total lymphocyte proportions and B cells, but significantly higher proportions of T cells and monocytes. There were also significantly more activated T cells, activated T helper cells and activated cytotoxic T cells (Table 6) (correlation coefficient of 0.630 for $CD4DR^+$ and of 0.661 for $CD8DR^+$ cells, Spearman's correlation analysis).

Discussion

Data illustrating the spectrum of spontaneous and experimentally induced diseases in humanized mice are very limited, and the situation is similar for the recipient NSG immunodeficient mice. Besides, detailed characterization of the morphological aspects of repopulation at tissue level is highly desirable to allow accurate correlation with the engraftment features obtained via FACS analysis. This study aimed to characterise the morphological phenotype of NSG mice and their humanized counterpart, the $CD34^+$ hu-NSG murine model, and to gather data on the most common background lesions in both types of mice. In addition, a comparative quantitative assessment was undertaken in the attempt to relate levels of human repopulation in the hemolymphatic organs of hu-NSG mice to FACS results obtained from the peripheral blood, as the latter is commonly used as a tool to determine the extent of humanization.

Full histological examination of a cohort of 48 NSG mice aged 3 to 6 months revealed a limited spectrum of background lesions, occurring with low severity. Salient changes were observed in lungs, kidneys, testes and adrenal glands and were all among those commonly encountered in other strains.[13,17,44] In addition, there was a very low prevalence of incidental inflammatory changes, without evidence of infectious conditions. This can likely be ascribed to housing of the mice under specific

pathogen free conditions as in general NSG mice are prone to infections because their immune system is compromised.[16]

Since the present study focused on young animals, it cannot provide data on potential spontaneous neoplastic processes that might develop with age.[47] Interestingly though, lymphoma was found in the thoracic cavity of a 6-month-old non-irradiated female NSG mouse, which could have originated from the thymus or the mediastinal lymph nodes. The tumor was predominantly composed of $CD3^+$, $CD4^+$ T cells and further characterized as a T cell lymphoblastic lymphoma. Hematopoietic neoplasms are reported to occur with low prevalence in NSG mice, in subjects older than 1 year,[16,47] due to the inactivation of IL-2Rγ, which plays an important role in the signalling pathways for B and T cell growth.[26] In the present case, it could be a spontaneous event that might have compensated for IL-2Rγ deficiency, and led to full manifestation of the NOD-scid background phenotype, which has been reported to frequently develop lymphoma.[41] Lymphoma, especially thymic lymphoma might also occur secondarily to irradiation, which is used to deplete mouse hematopoetic cells prior to human cell engraftment, or insertional mutagenesis resulting from gene editing therapeutic products. Hence, it is crucial to report on the occurrence of such tumors in untreated NSG mice at an age when they are used in transplantation experiments, to build an accurate historical database.

All NSG mice in the present study showed poorly developed lymphoid organs, lacking the typical lymphoid tissue architecture. This has previously been reported as a feature in the lymphoid organs of several immunodeficient murine lines, including NSG mice, whose genetic manipulation leads to severe impairment of immune functions.[7,47,49,52] However, we observed small or moderately sized periarteriolar clusters of $mCD45^+$ cells in the spleen of numerous NSG mice, a feature that has to our knowledge not been reported yet. Cells in these clusters did not express more

549 specific lymphocyte or macrophage markers, so further work is needed to assess
550 their exact nature and whether they represent early lymphoid precursors, dendritic or
551 myeloid subsets. According to the experience of the authors, these aggregates can
552 complicate the histologic interpretation of NSG mice engrafted with human
553 hematopoietic cells or administered cell-based therapy products, which might have
554 morphological features similar to these native cells in HE-stained sections. Another
555 interesting observation was that, like the bone marrow in *scid* and other
556 immunodeficient mouse lines, the bone marrow of NSG mice did not show major
557 histological abnormalities in the hematopoetic cell component.[14]
558 The comprehensive histological screening of hu-NSG mice, i.e. NSG mice engrafted
559 with human $CD34^+$ HSC, revealed a spectrum of spontaneous lesions similar to that
560 observed in naïve NSG mice. However, the mice additionally exhibited changes that
561 can be ascribed to either the preconditioning irradiation and/or the engraftment of
562 human hematopoietic cells.
563 Among the lesions potentially related to perinatal total body irradiation, to which the
564 *scid* mutation of NSG mice renders them particularly sensitive,[5] were nephropathy,
565 ovarian atrophy and ocular changes. All three are well-known complications of
566 radiation exposure in humans.[3,12] Radiation nephropathy has also been described in
567 different preclinical species including mice.[12] In both humans and laboratory animals
568 it represents a late onset, adverse event following external beam irradiation or
569 radionuclide therapy, characterized by concurrent injury to glomerular and tubular
570 compartments.[12,40] In the present study it was observed with low frequency and
571 severity, which suggests an early stage of the disease in the still-young hu-NSG
572 mice. At this early stage, radiation-induced lesions can be hard to differentiate from
573 tubular basophilia and the early changes that can occur in the context of chronic

574 progressive nephropathy, a common degenerative spontaneous disease in the
575 kidneys of mice and rats.[17]
576 So far, both ovarian atrophy and retinal changes have only been sporadically
577 reported as radiation-induced alterations in animal models, and the present report is
578 the first of such lesions in hu-NSG mice undergoing perinatal preconditioning.
579 Interestingly, both types of changes occurred with high prevalence and severity,
580 indicating a high sensitivity of ovaries and retina of these mice to irradiation. It is
581 known that the germline cells in the ovary are highly susceptible to radiation damage
582 and that accelerated reproductive aging can occur when the follicle pool, which is
583 finite and non-renewable, is damaged due to irradiation.[1] From the present findings it
584 could be speculated that radiation-induced damage of the female germ cells at an
585 early prepubertal stage might cause loss of ovarian reserve, which then manifests as
586 atrophy of the gonads and lack of cyclical changes in uterus and vagina.
587 Interestingly, there were no substantial microscopic changes in the testes of hu-NSG
588 mice, suggesting that the irradiation procedure did not affect the male germline. This
589 difference might be due to different radiation exposure or reduced sensitivity of the
590 male gonadal tissues in the postnatal period, as previously reported.[15]
591 Radiation retinopathy in humans encompasses a number of retinal changes following
592 exposure to radiation from any source, typically external beam radiation exposure in
593 patients affected by tumors of the nasopharynx, sinus or orbita.[3] In animal models,
594 complications of ocular radiation have been reported as rare, most frequently
595 manifesting as cataracts, which also occurred in this study with low prevalence and
596 low severity.[43] The retinal lesions observed in our mouse cohort suggest a perinatal
597 arrest of the retinal development, allowing only the neuroblastic layer and the
598 ganglion cell layer to be identified.[59] To our knowledge, these retinal lesions have not
599 been previously reported in mice that have undergone total body irradiation.

Extensive photoreceptor loss and impaired retinal development in the hu-NSG mice might therefore be linked to radiation exposure in the perinatal period, when cell proliferation is still ongoing in the retina as part of the postnatal development process. Nonetheless, a more thorough investigation of the retinal changes was beyond the scope of the present study, as it would require dedicated long-term studies with multiple endpoints and multiple radiation quantities. Notably though, researchers should be aware of potential impaired vision resulting from the retinal lesions. Impaired retinal development affects predominantly the outer layers, hence resembling outer retinal atrophy, from which it needs to be differentiated. The latter is characterized by loss of photoreceptors and is caused by a number of factors, including aging and phototoxicity.[42]

The changes that can be ascribed to the engraftment of human hematopoetic cells are represented by granulomatous inflammatory infiltrates of almost exclusively human origin that were found in multiple organs of around 20% of hu-NSG mice. The absence of microorganisms and foreign material and the dominance of macrophages and $CD4^+$ T cells suggest either an uncontrolled proliferation of activated human immune cells and/or an underlying human-anti-mouse immunopathological process. Granulomatous infiltrates containing hemosiderin-laden macrophages are reminiscent of post-transplant hemophagocytic lymphohistiocytosis (HLH), an hyperinflammatory condition driven by hypercytokinemia and triggered, for example, by transplantation of HSC.[46] The disease has been reproduced in perforin-deficient mice infected with lymphocytic choriomeningitis virus[27] and in humanized mice following experimental infection with EBV.[48] More recently, it has also been described in NSG-SGM3 mice without human thymus, engrafted with human $CD34^+$ fetal liver cells.[63] The infiltrates in these mice were similar to the lymphohistiocytic infiltrates observed in hu-NSG mice in our study and were not present in NSG mice. However,

in general, the inflammatory infiltrates in CD34+ HSC humanized NSG mice as in our study ~~are characterized by less prominent hemophagocytosis~~ exhibit only occasional hemosiderin-laden macrophages and, in the lungs, have a predominantly lymphocytic rather than histiocytic/granulomatous character. In the liver, inflammatory foci were predominantly present in portal areas, but seemed not to target the biliary ducts; the latter is a striking feature of GvHD in humans. To date, a number of studies have reported multiorgan infiltrates of lymphocytes and macrophages, occasionally with epithelioid macrophages and giant cells, as a manifestation of GvHD in humanized mice,[11,18,28,34,53] and report GvHD as a major cause of morbidity in studies employing humanized mice.[21,28] Considering that Yoshihara and co-authors consider lymphohistiocytic infiltrates with a prominent hemophagocytic component as indicative of HLH rather than GvHD it is also possible that both conditions manifest concurrently in the same model. This seems likely in our murine model, where the inflammatory processes observed in the skin of a few mice, i.e. an interface dermatitis with vacuolation and apoptosis of keratinocytes in the basal layer of hair follicles, closely resemble the typical manifestation of chronic GvHD in human patients, while the multisystemic granulomatous infiltration would rather suggest an uncontrolled proliferation of human macrophages driven by an excess in cytokines, as in HLH.[27,46] In the absence of additional evidence pointing toward one entity or the other, we feel that other methodological approaches, such as T cell receptor repertoire analysis and quantification of plasma and tissue cytokine levels are needed to provide more insight into the exact nature and pathogenesis of these inflammatory lesions.[11,21,51]

Since mice affected by granulomatous inflammation do not reach the experimental end-point they are often excluded from the analysis. Thus, the frequency of the respective pathological changes, whose underlying cause is ascribed to GvHD or

652 HLH, is rarely reported.[3] In the present study, thirteen mice showed weight reduction
653 or clinical signs and all but one of them exhibited granulomatous inflammation, with
654 more males found to be affected (21%) than females (11%). These data indicate that
655 monitoring of weight loss and clinical signs can identify the majority of mice with
656 these specific pathological changes. Still, some mice with only few and mild lesions
657 that can only be detected by histological examination may not be identified based on
658 clinical signs, yet these may show an aberrant immunological response of the
659 engrafted human cells in different types of experiments. It is important to highlight
660 though that the prevalence and features of granulomatous inflammation reported
661 here might solely apply to the model employed in our study, as there is growing
662 evidence that the incidence and severity of inflammatory lesions varies extensively
663 across experiments depending on the source, number and manipulation of human
664 donor cells employed and the features of the recipient host system (e.g. strain
665 susceptibility, environmental features and preconditioning protocols involving
666 irradiation or chemotherapy).[20,36]
667 In the present study, the *in situ* detection of human and murine cells in the
668 hemolymphatic tissues provided information on the extent and distribution of homing
669 of graft and host leukocytes after humanization with $CD34^+$ HSC. We observed that
670 the mouse component ($mCD45^+$ cells) generally decreased with humanization of the
671 animal, even though the difference was not statistically significant. This phenomenon
672 cannot be explained without further studies employing larger numbers of animals. It
673 could simply be a consequence of irradiation; alternatively, it is possible that the
674 introduction of human cells leads to a reduced proliferation of the murine leukocytes.
675 Both FACS data and the image analysis of tissue sections of hemolymphatic organs
676 suggested that the extent of $hCD45^+$ repopulation was highly variable among the
677 engrafted animals. The reason for this is not clear, but pre-treatment, injection route,

and source of HSCs will inevitably have an impact on the inter- and intra-experimental variability of engraftment. This makes comparisons across different models difficult, even when experimental conditions vary only slightly. Human cells showed a variable distribution in the different organs. In the spleen, $hCD45^+$ cells formed aggregates reminiscent of the white pulp of immunocompetent mice, despite the absence of discernible PALS and lymphoid follicle organisation. The thymus of hu-NSG mice was variably repopulated by human T cells, providing further evidence of some functional homing of the lymphocytes; however, the typical architecture was not observed. In the lymph nodes, however, there was no evidence of a cell type-specific arrangement. It has previously been suggested that the genetic background of the mice is responsible for the lack of the typical architecture in the lymphoid organs, as γ_c deficiency compromises IL-7-dependent lymphoid tissue inducer cell development.[33] The architecture is crucial for the proper functionality of the immune system,[39] and it has been suggested that the poorly organized lymphoid organs are a limiting factor in the humoral immune response of humanized mice.[61] Repopulation of the bone marrow seems to be less complicated; in - bone marrows free of inflammatory lesions, all cell types appeared to home effectively.

The present study also investigated the correlation between the pattern and extent of reconstitution in the lymphoid organs by human leukocytes and the results of the FACS analysis on peripheral blood. The FACS analysis revealed a high variability in reconstitution between different animals, and similarly the actual distribution of $hCD45^+$ in the lymphoid organs of an individual can be quite variable. Upon pairing the obtained FACS data of the reconstitution 3 to 6 months after human HSC injection with the morphological analysis of the lymphoid organs it became evident that a high reconstitution based on analysis of blood does not necessarily correlate with a high repopulation at the tissue level. In the efficiently humanized mice there

was no significant correlation between the level of circulating hCD45$^+$ cells and the number of hCD45$^+$ cells in the organs, whereas a significant correlation was seen in the inefficiently humanized animals. This significance may be due to the low hCD45$^+$ cell levels in all the compartments and thus a lower variability.

In the animals affected by granulomatous infiltrates the proportion of human leukocytes and lymphocytes in the blood were significantly lower compared to mice that did not exhibit evidence of such inflammatory changes. This might result from migration of human leukocytes from the blood stream to the sites of injury, similarly to what occurs in infections and sepsis,[55] and by compromised hematopoietic function due to granulomatous lesions in the bone marrow, as was visible in the histological evaluation of some of the animals. However, compared to the cohort not affected by granulomatous inflammation, those affected by this process had a significantly higher proportion of T cells in the blood including higher numbers of activated T cells, activated T helper cells and activated cytotoxic T cells. The increased numbers of T cells fit with the central role of effector graft donor T cells in driving these post-transplant pathological processes.[10,36] Moreover, the granulomatous lesions in the bone marrow of affected animals were dominated by MHC II-positive cells, and also activated T cells are known to express this surface antigen.[30] This hypothesis is supported by a study that shows an increase in the proportion and extent of fluctuation of CD3$^+$CD4$^+$CD8β$^+$ T cells.[10]

Identification of an increase in T cells, primarily activated helper T cells in the FACS data might help to spot individual mice affected by subclinical inflammatory lesions, which could then be confirmed via the histological examination of typically affected organs such as the bone marrow, liver and kidneys.

Acknowledgements

The authors wish to thank the technical staff of the Histology Laboratory, Laboratory for Animal Model Pathology, Institute of Veterinary Pathology, Vetsuisse Faculty, University of Zurich, for excellent technical support.

CM is supported by Cancer Research Switzerland (KFS-4091-02-2017), KFSP-Precision^{MS} of the University of Zurich, the Vontobel Foundation, the Baugarten Foundation, the Sobek Foundation, the Swiss Vaccine Research Institute, Roche, ReiThera and the Swiss National Science Foundation (310030B_182827 and CRSII5_180323).

References

1 Adriaens I, Smitz J, Jacquet P. The current knowledge on radiosensitivity of ovarian follicle development stages. *Hum Reprod Update*. 2009;3;359–377.

2 Antsiferova O, Müller A, Rämer PC, et al. Adoptive transfer of EBV specific CD8+ T cell clones can transiently control EBV infection in humanized mice. *PLoS Pathog*. 2014;8;e1004333.

3 Bawankar P, Barman M, Bhattacharjee H, Soibam R, Paulbuddhe V. Radiation retinopathy after external beam irradiation for nasopharyngeal carcinoma: A case report and review of the literature. *Practical Radiation Oncology*. 2018;6;366–368.

4 Borges HL, Chao C, Xu Y, Linden R, Wang JYJ. Radiation-induced apoptosis in developing mouse retina exhibits dose-dependent requirement for ATM phosphorylation of p53. *Cell Death and Differentiation*. 2004;5;494.

5 Bosma MJ, Carroll AM. The SCID mouse mutant: definition, characterization, and potential uses. *Annu Rev Immunol*. 1991;323–350.

6 Braga-Tanaka I, Tanaka S, Kohda A, et al. Experimental studies on the biological effects of chronic low dose-rate radiation exposure in mice: overview of the studies at the Institute for Environmental Sciences. *Int J Radiat Biol*. 2018;5;423–433.

7 Brehm MA, Cuthbert A, Yang C, et al. Parameters for establishing humanized mouse models to study human immunity: analysis of human hematopoietic stem cell engraftment in three immunodeficient strains of mice bearing the IL2rgamma(null) mutation. *Clin Immunol*. 2010;1;84–98.

8 Brehm MA, Shultz LD, Luban J, Greiner DL. Overcoming current limitations in humanized mouse research. *J Infect Dis*. 2013;S125-30.

9 Brehm MA, Wiles MV, Greiner DL, Shultz LD. Generation of improved humanized mouse models for human infectious diseases. *J Immunol Methods*. 2014;3–17.

10 Brinkman RR, Gasparetto M, Lee S-JJ, et al. High-content flow cytometry and temporal data analysis for defining a cellular signature of graft-versus-host disease. *Biol Blood Marrow Transplant*. 2007;6;691–700.

11 Chandra S, Cristofori P, Fonck C, O'Neill CA. Ex Vivo Gene Therapy: Graft-versus-host Disease (GVHD) in NSG™ (NOD.Cg-Prkdcscid Il2rgtm1Wjl/SzJ) Mice Transplanted with CD34+ Human Hematopoietic Stem Cells. *Toxicol Pathol*. 2019;192623319844484.

12 Cohen EP, Robbins MEC. Radiation nephropathy. *Semin Nephrol*. 2003;5;486–499.

13 Creasy D, Bube A, Rijk E de, et al. Proliferative and nonproliferative lesions of the rat and mouse male reproductive system. *Toxicol Pathol*. 2012;6 Suppl;40S-121S.

14 Custer RP, Bosma GC, Bosma MJ. Severe combined immunodeficiency (SCID) in the mouse. Pathology, reconstitution, neoplasms. *Am J Pathol*. 1985;3;464–477.

15 Forand A, Messiaen S, Habert R, Bernardino-Sgherri J. Exposure of the mouse perinatal testis to radiation leads to hypospermia at sexual maturity. *Reproduction*. 2009;3;487–495.

16 Foreman O, Kavirayani AM, Griffey SM, Reader R, Shultz LD. Opportunistic bacterial infections in breeding colonies of the NSG mouse strain. *Vet Pathol*. 2011;2;495–499.

17 Frazier KS, Seely JC, Hard GC, et al. Proliferative and nonproliferative lesions of the rat and mouse urinary system. *Toxicol Pathol*. 2012;4 Suppl;14S-86S.

18 Fujii H, Luo Z-J, Kim HJ, et al. Humanized Chronic Graft-versus-Host Disease in NOD-SCID il2rγ-/- (NSG) Mice with G-CSF-Mobilized Peripheral Blood Mononuclear Cells following Cyclophosphamide and Total Body Irradiation. *PLoS ONE*. 2015;7;e0133216.

19 Gille C, Orlikowsky TW, Spring B, et al. Monocytes derived from humanized neonatal NOD/SCID/IL2Rγ(null) mice are phenotypically immature and exhibit functional impairments. *Hum Immunol*. 2012;4;346–354.

20 Gorin N-C, Piantadosi S, Stull M, Bonte H, Wingard JR, Civin C. Increased risk of lethal graft-versus-host disease-like syndrome after transplantation into NOD/SCID mice of human mobilized peripheral blood stem cells, as compared to bone marrow or cord blood. *J Hematother Stem Cell Res*. 2002;2;277–292.

21 Greenblatt MB, Vrbanac V, Vbranac V, et al. Graft versus host disease in the bone marrow, liver and thymus humanized mouse model. *PLoS ONE*. 2012;9;e44664.

22 Greiner DL, Hesselton RA, Shultz LD. SCID Mouse models of human stem cell engraftment. *Stem Cells*. 1998;3;166–177.

23 Ishikawa F, Yasukawa M, Lyons B, et al. Development of functional human blood and immune systems in NOD/SCID/IL2 receptor γ chainnull mice. *Blood*. 2005;5;1565–1573.

24 Ito M, Hiramatsu H, Kobayashi K, et al. NOD/SCID/gamma©(null) mouse: an excellent recipient mouse model for engraftment of human cells. *Blood*. 2002;9;3175–3182.

25 Ito M, Kobayashi K, Nakahata T. NOD/Shi-scid IL2rgamma(null) (NOG) mice more appropriate for humanized mouse models. *Curr Top Microbiol Immunol*. 2008;53–76.

26 Ito R, Takahashi T, Katano I, Ito M. Current advances in humanized mouse models. *Cell Mol Immunol*. 2012;3;208–214.

27 Jordan MB, Hildeman D, Kappler J, Marrack P. An animal model of hemophagocytic lymphohistiocytosis (HLH): CD8+ T cells and interferon gamma are essential for the disorder. *Blood*. 2004;3;735–743.

28 King MA, Covassin L, Brehm MA, et al. Human peripheral blood leucocyte non-obese diabetic-severe combined immunodeficiency interleukin-2 receptor gamma chain gene mouse model of xenogeneic graft-versus-host-like disease and the role of host major histocompatibility complex. *Clin Exp Immunol*. 2009;1;104–118.

29 Koboziev I, Jones-Hall Y, Valentine JF, Webb CR, Furr KL, Grisham MB. Use of Humanized Mice to Study the Pathogenesis of Autoimmune and Inflammatory Diseases. *Inflamm Bowel Dis*. 2015;7;1652–1673.

30 Lal G, Shaila MS, Nayak R. Activated mouse T-cells synthesize MHC class II, process, and present morbillivirus nucleocapsid protein to primed T-cells. *Cell Immunol*. 2005;2;133–145.

31 Lan P, Tonomura N, Shimizu A, Wang S, Yang Y-G. Reconstitution of a functional human immune system in immunodeficient mice through combined human fetal thymus/liver and CD34+ cell transplantation. *Blood*. 2006;2;487–492.

32 Lang J, Kelly M, Freed BM, et al. Studies of lymphocyte reconstitution in a humanized mouse model reveal a requirement of T cells for human B cell maturation. *J Immunol*. 2013;5;2090–2101.

33 Li Y, Masse-Ranson G, Garcia Z, et al. A human immune system mouse model with robust lymph node development. *Nat Methods*. 2018;8;623–630.

34 Lockridge JL, Zhou Y, Becker YA, et al. Mice engrafted with human fetal thymic tissue and hematopoietic stem cells develop pathology resembling chronic graft-versus-host disease. *Biol Blood Marrow Transplant*. 2013;9;1310–1322.

35 Lysenko V, McHugh D, Behrmann L, et al. Humanised mouse models for haematopoiesis and infectious diseases. *Swiss Med Wkly*. 2017;w14516.

36 MacDonald KPA, Hill GR, Blazar BR. Chronic graft-versus-host disease: biological insights from preclinical and clinical studies. *Blood*. 2017;1;13–21.

37 Mähler Convenor M, Berard M, Feinstein R, et al. FELASA recommendations for the health monitoring of mouse, rat, hamster, guinea pig and rabbit colonies in breeding and experimental units. *Lab Anim*. 2014;3;178–192.

38 Morse HC, Anver MR, Fredrickson TN, et al. Bethesda proposals for classification of lymphoid neoplasms in mice. *Blood*. 2002;1;246–258.

39 Pearson T, Shultz LD, Miller D, et al. Non-obese diabetic-recombination activating gene-1 (NOD-Rag1 null) interleukin (IL)-2 receptor common gamma chain (IL2r gamma null) null mice: a radioresistant model for human lymphohaematopoietic engraftment. *Clin Exp Immunol*. 2008;2;270–284.

40 Pellegrini G, Siwowska K, Haller S, et al. A short-term biological indicator for long-term kidney damage after radionuclide therapy in mice. *Pharmaceuticals (Basel)*. 2017;2.

41 Prochazka M, Gaskins HR, Shultz LD, Leiter EH. The nonobese diabetic scid mouse: model for spontaneous thymomagenesis associated with immunodeficiency. *Proc Natl Acad Sci U S A*. 1992;8;3290–3294.

42 Ramos MF, Baker J, Atzpodien E-A, et al. Nonproliferative and proliferative lesions of the rat and mouse special sense organs (ocular [eye and glands], olfactory and otic). *J Toxicol Pathol*. 2018;3 Suppl;97S-214S.

43 Ramos MS, Echegaray JJ, Kuhn-Asif Dacvo S, et al. Animal models of radiation retinopathy - From teletherapy to brachytherapy. *Exp Eye Res*. 2019.

44 Renne R, Brix A, Harkema J, et al. Proliferative and nonproliferative lesions of the rat and mouse respiratory tract. *Toxicol Pathol*. 2009;7 Suppl;5S-73S.

45 Rongvaux A, Willinger T, Martinek J, et al. Development and function of human innate immune cells in a humanized mouse model. *Nat Biotechnol*. 2014;4;364–372.

46 Sandler RD, Carter S, Kaur H, Francis S, Tattersall RS, Snowden JA. Haemophagocytic lymphohistiocytosis (HLH) following allogeneic haematopoietic stem cell transplantation (HSCT)-time to reappraise with modern diagnostic and treatment strategies? *Bone Marrow Transplant*. 2020;2;307–316.

878 47 Santagostino SF, Arbona RJR, Nashat MA, White JR, Monette S. Pathology of
879 aging in NOD scid gamma female mice. *Vet Pathol*. 2017;5;855–869.
880 48 Sato K, Misawa N, Nie C, et al. A novel animal model of Epstein-Barr virus-
881 associated hemophagocytic lymphohistiocytosis in humanized mice. *Blood*.
882 2011;21;5663–5673.
883 49 Seymour R, Sundberg JP, Hogenesch H. Abnormal lymphoid organ
884 development in immunodeficient mutant mice. *Vet Pathol*. 2006;4;401–423.
885 50 Shackelford C, Long G, Wolf J, Okerberg C, Herbert R. Qualitative and
886 quantitative analysis of nonneoplastic lesions in toxicology studies. *Toxicol*
887 *Pathol*. 2002;1;93–96.
888 51 Shultz LD, Brehm MA, Garcia-Martinez JV, Greiner DL. Humanized mice for
889 immune system investigation: progress, promise and challenges. *Nat Rev*
890 *Immunol*. 2012;11;786–798.
891 52 Shultz LD, Lyons BL, Burzenski LM, et al. Human lymphoid and myeloid cell
892 development in NOD/LtSz-scid IL2R null mice engrafted with mobilized human
893 hemopoietic stem cells. *J Immunol*. 2005;10;6477–6489.
894 53 Sonntag K, Eckert F, Welker C, et al. Chronic graft-versus-host-disease in
895 CD34(+)-humanized NSG mice is associated with human susceptibility HLA
896 haplotypes for autoimmune disease. *J Autoimmun*. 2015;55–66.
897 54 Strowig T, Chijioke O, Carrega P, et al. Human NK cells of mice with
898 reconstituted human immune system components require preactivation to
899 acquire functional competence. *Blood*. 2010;20;4158–4167.
900 55 Tanaka J, Sato T, Jones RT, Trump BF, Cowley RA. The pathophysiology of
901 septic shock: responses to different doses of live Escherichia coli injection in
902 rats. *Adv Shock Res*. 1983;101–114.

56 Tanaka S, Saito Y, Kunisawa J, et al. Development of mature and functional human myeloid subsets in hematopoietic stem cell-engrafted NOD/SCID/IL2rγKO mice. *J Immunol*. 2012;12;6145–6155.

57 Theocharides APA, Rongvaux A, Fritsch K, Flavell RA, Manz MG. Humanized hemato-lymphoid system mice. *Haematologica*. 2016;1;5–19.

58 Unanue ER. Antigen presentation in the autoimmune diabetes of the NOD mouse. *Annu Rev Immunol*. 2014;579–608.

59 van Cruchten S, Vrolyk V, Perron Lepage M-F, et al. Pre- and postnatal development of the eye: a species comparison. *Birth Defects Res*. 2017;19;1540–1567.

60 Vuyyuru R, Patton J, Manser T. Human immune system mice: current potential and limitations for translational research on human antibody responses. *Immunol Res*. 2011;2-3;257–266.

61 Walsh NC, Kenney LL, Jangalwe S, et al. Humanized mouse models of clinical disease. *Annu Rev Pathol*. 2017;187–215.

62 Yahata T, Ando K, Nakamura Y, et al. Functional human T lymphocyte development from cord blood CD34+ cells in nonobese diabetic/Shi-scid, IL-2 receptor null mice. *J Immunol*. 2002;1;204–209.

63 Yoshihara S, Li Y, Xia J, Danzl N, Sykes M, Yang Y-G. Posttransplant hemophagocytic lymphohistiocytosis driven by myeloid cytokines and vicious cycles of T-cell and macrophage activation in humanized mice. *Front Immunol*. 2019;186.

64 Zhang B, Duan Z, Zhao Y. Mouse models with human immunity and their application in biomedical research. *J Cell Mol Med*. 2008;6;1043–1058.

928 **Figure legends**

929 **Figures 1-3**. Radiation exposure (one-time irradiation with 1Gy at the age of 1-6
930 days), hu-NSG mouse. Hematoxylin and eosin. **Figure 1**. Kidney. Radiation
931 nephropathy. Cortical tubules are collapsed (arrows in main image and top inset).
932 Inset bottom: There is deposition of proteinaceous material and reduced number of
933 capillaries in a glomerulus (arrowhead). **Figure 2**. Eye. Most structures of the retina
934 cannot be identified. There appears to be an irregular ganglion cell layer (GCL) and a
935 defined neuroblastic layer (NBL) of up to six cell layers. **Figure 3**. Ovary. The ovary is
936 small and devoid of follicles and corpora lutea.
937
938 **Figures 4-7**. Spleen. **Figure 4**. NSG mouse. **a**. There are no distinct white pulp
939 structures. Occasional aggregates of round cells form structures reminiscent of
940 periarteriolar lymphoid sheaths (PALS) (arrows). The red pulp is cell-rich, mainly due
941 to extramedullary hematopoiesis. Inset: PALS-like structure (arrowhead: artery).
942 Hematoxylin and eosin (HE). **b**. The PALS-like structures are comprised of $mCD45^+$
943 cells that aggregate around a splenic arteriole (arrowhead). Numerous $mCD45^+$ cells
944 are also randomly distributed in the red pulp. Immunohistochemistry, hemalaun
945 counterstain. **Figure 5**. hu-NSG mouse. **a**. The white pulp is prominent, with large
946 aggregates of lymphoid cells clustering around arterioles (arrowhead), consistent with
947 PALS. The red pulp is cell-rich, with abundant extramedullary hematopoiesis. HE. **b**.
948 Murine leukocytes ($mCD45^+$) are rare (arrowheads). Inset: Higher magnification of
949 $mCD45^+$ cells (arrowheads). Immunohistochemistry, hemalaun counterstain. **c**.
950 Human leukocytes ($hCD45^+$) form the PALS-like aggregates and are also distributed
951 in moderate number throughout the red pulp (hCD45-positive cell fraction area of
952 13.4%). Immunohistochemistry, hemalaun counterstain. **Figure 6**. Boxplot presenting
953 the area in the spleen of NSG and hu-NSG mice covered by $mCD45^+$ cells (mCD45

positive cell fraction area in %). There is a trend toward a lower percentage of mCD45$^+$ cells in hu-NSG mice, however, the difference is not statistically significant ($p = 0.148$). **Figure 7**. hu-NSG mouse. **a**. The PALS-like structures around the arteries are mainly comprised of T cells (CD3$^+$). **b**. B cells (CD20$^+$) arrange around the PALS-like structures, without forming clear follicles. Immunohistochemistry, hemalaun counterstain.

Figures 8-10. Lymph nodes. **Figure 8**. Mesenteric lymph node, NSG mouse. **a**. The lymph node is very small. The inset shows that it is mainly represented by a meshwork of fibrous tissue (reticular stroma), with low numbers of embedded leukocytes (arrowheads). Hematoxylin and eosin (HE) . **b**. The lymph node contains only few mCD45$^+$ leukocytes. Immunohistochemistry, hemalaun counterstain. **Figure 9**. Mesenteric lymph node, hu-NSG mouse (well repopulated; hCD45-positive cell fraction area of 43.2%). **a**. The lymph node exhibits high cellularity, although no clear follicular and paracortical structures are identified. HE. **b, c**. The repopulating cells are B cells (b, CD20$^+$) and T cells (c, CD3$^+$) that seem to cluster to some extent but do not form follicles or T cell zones. **d**. Almost all cells are hCD45-positive. Immunohistochemistry, hemalaun counterstain. **Figure 10**. Boxplot presenting the area in the lymph nodes of NSG and hu-NSG mice covered by mCD45$^+$ cells (mCD45 positive cell fraction area in %). There is a trend toward a lower percentage of mCD45$^+$ cells in hu-NSG mice, however, this is not statistically significant ($p = 0.059$).

Figures 11-14. Thymus. **Figures 11, 12**. NSG mouse. **Figure 11**. Hypoplastic thymus without defined cortex and medulla, devoid of lymphocytes and with a large cyst (*). Hematoxylin and eosin (HE). **Figure 12**. Leukocytes (mCD45$^+$) are found in

low numbers and randomly distributed (arrowhead). Immunohistochemistry, hemalaun counterstain. **Figure 13**. hu-NSG mouse. **a**. Cortex and medulla cannot be identified, but there is a moderate cellularity with numerous disseminated lymphoid cells. HE. **b**. Murine leukocytes (mCD45$^+$) are disseminated in low numbers. **c**. The vast majority of the lymphoid cells are hCD45$^+$ human leukocytes, confirming repopulation (hCD45 positive cell fraction area of 42.6%). Immunohistochemistry, hemalaun counterstain. **Figure 14**. Boxplot presenting the area in the thymus of NSG and hu-NSG mice covered by mCD45$^+$ cells (mCD45 positive cell fraction area in %). There is no significant difference in the percentage of mCD45$^+$ cells between the two groups of mice ($p = 0.533$).

Figures 15-17. Femoral bone marrow. **Figure 15**. NSG mouse. **a**. The bone marrow is cell-rich; all hematopoietic cells are represented. Hematoxylin and eosin (HE). **b**. There are abundant mCD45$^+$ leukocytes. Immunohistochemistry, hemalaun counterstain. **Figure 16**. hu-NSG mouse. **a**. The bone marrow is highly cellular; all hematopoietic cell lineages are represented. HE. **b**. The number of mCD45$^+$ cells is low, positive cells are often apoptotic (arrowheads, also in inset). **c**. The majority of cells are hCD45-positive. Immunohistochemistry, hemalaun counterstain. **Figure 17**. Boxplot presenting the area in the bone marrow of NSG and hu-NSG mice covered by mCD45$^+$ cells (mCD45 cell fraction area in %). A significantly ($p = 0.006$) lower percentage of mCD45$^+$ cells is present in hu-NSG mice.

Figures 18-24. Granulomatous inflammation, hu-NSG mouse. **Figure 18**. Liver. There are multifocal inflammatory infiltrates, mainly arranged around portal areas. *, portal vein. Hematoxylin and eosin (HE). **Figure 19**. Liver. Cells in the focal infiltrates predominantly have the morphology of macrophages and lymphocytes (a, HE) and

almost all are Ku80-positive (b), confirming their human origin. These cells include numerous T cells (c, $CD3^+$) and fewer B cells (d, $CD20^+$). Immunohistochemistry, hemalaun counterstain. **Figure 20**. Bone marrow. **a**. Within the hematopoietic tissue are variably sized aggregates of larger mononuclear cells (arrows). HE. **b**. The majority of cells in such focal aggregates express MHC II, suggesting that there are abundant macrophages and activated lymphocytes. Immunohistochemistry, hemalaun counterstain. **Figures 21, 22**. Spleen. The red pulp is widely replaced by large granulomatous infiltrates (Fig. 21, arrows) including epithelioid cells (Fig. 22, arrowhead) and multinucleated cells (Fig. 22, arrow). HE. **Figures 23, 24**. Cervical lymph node. The normal architecture is widely replaced by granulomatous infiltrates (*). HE.

.

Figures 25-28. Comparison of efficiently humanized mice (hu-NSG(e), Figures 25 and 27) and inefficiently humanized mice (hu-NSG(i), Figures 26 and 28). **Figures 25, 26**. Proportion of human cells in the blood ($hCD45^+$, FACS) and lymphoid organs ($hCD45^+$, immunohistochemistry). Each symbol and line represents one individual. Note the large variability among the different individuals but also among different organs of a single individual. Grouping of the mice followed FACS analysis (cut off 15% hCD45). Lymph node values include the average of all detected lymph nodes in each animal (axillary, cervical and mesenteric). Animals with granulomatous inflammatory infiltrates are marked with an asterisk. Only organs without lesions were evaluated. **Figures 27, 28**. Proportion of human cells in the blood ($hCD45^+$, FACS) and bone marrow ($Ku80^+$, immunohistochemistry). Each symbol and line represents one individual. Note the large variability among the different individuals but also among different organs of a single individual, especially in the group of hu-NSG(i)

mice. Animals with granulomatous inflammatory processes are marked with an asterisk in Figures 25 and 26.

Supplemental figures

Figures S1, 2. T cell lymphoblastic lymphoma, thoracic cavity, NSG mouse, 6 months, female. **Figure S1**. Thoracic mass composed of a monomorphic neoplastic cell population that also infiltrates the adjacent mediastinal adipose tissue. HE stain. **Figure S2**. **a**. Neoplastic cells are arranged in tightly packed sheets and display scant amphophilic cytoplasm, round nuclei, and moderate anisocytosis. There are several mitotic (arrows) and apoptotic (arrowheads) cells. HE stain. **b**. The vast majority of neoplastic cells express the pan T cell marker CD3. **c**. Neoplastic cells are also CD4 positive (pink reaction along the cell border), but CD8 negative (no cells with blue reaction along the cell border). Immunohistochemistry, hemalaun counterstain.